University of Naples “Federico II”

School of Medicine and Surgery
Department of Public Health

Doctoral School in
Public Health and Preventive Medicine
XXXIII cycle

Thyroid hormone orchestrates the epithelial carcinogenesis through the NANOG-D2-T3-ZEB1 axis

TUTOR
Prof. Domenico SALVATORE

STUDENT
Dr. Annarita NAPPI

COORDINATOR
Prof. Giancarlo TRONCONE

ACADEMIC YEAR
2019/2020

INDEX

1. Summary

1.1 Thyroid hormone orchestrates the epithelial carcinogenesis through the NANOG-D2-T3-ZEB1 axis

Keratinocyte carcinomas (KCs), also known as non-melanocytic skin cancers (NMSCs), are the most common cutaneous malignancies diagnosed in fair-skinned populations. Molecular, epidemiologic, and clinical studies have led to understanding of the cellular events that occur during skin tumorigenesis and have provided new strategies for treatment and prevention of KCs. Genomic analyses have uncovered high-risk susceptibility genes, and somatic events that underlie common pathways important in KC tumorigenesis. Moreover, an emerging role for the endocrine therapy in the treatment of skin cancer has also been recognized in recent years. In this context, thyroid hormones (THs) are key endocrine regulators, whose action is critical both in physiological and pathological conditions, as in the case of the two most common subtypes of NMSC, basal cell carcinoma (BCC) and cutaneous squamous cell carcinoma (cSCC).

In the target tissues THs availability is regulated by the concerted actions of the TH-activating and inactivating enzymes, namely type 2 and type 3 deiodinases (D2 and D3), which act as a cell-specific pre-receptor mechanisms to control TH signaling independently of circulating levels of THs.

In the last decade, our group provided the evidence of a functional link between TH, its activating/inactivating enzymes, D2 and D3, and cancer formation. In particular, we demonstrated that: i) type 3 deiodinase (D3) enhances the proliferation of normal and malignant keratinocytes (1); ii) in the basal cell carcinoma (BCC) D3 is under the control of sonic hedgehog and is highly expressed in the early phases of tumorigenesis (2); iii) the microRNA-21 up-regulates D3 thereby reducing the TH level in BCC (3); iv) the concerted action of type 2 and type 3 deiodinases regulates the cell cycle and survival of basal cell carcinoma cells (4).

While the role of D3 has been investigated in the growth and differentiation of keratinocytes, both in pathological and in cancerous skin contexts, the effective role of TH D2-produced in the cancer progression was never been clarified. In this PhD program, we investigated the functional implication of D2 in KCs, identifying a comprehensive mechanistic insights into the regulation of D2 in cutaneous tumors (4). Elucidating the functional role of THs and tissue-specific modulation of deiodinases in tumorigenesis is crucial for the use of hormonal regulation as a new tool in a therapeutic context.

2. Introduction

2.1 Thyroid hormone action and deiodinases

Thyroid hormones (THs), thyroxine (T4) and triiodothyronine (T3), are pleiotropic agents that regulate the metabolism and homeostasis of many tissues in vertebrates (5). In the bloodstream, the steady-state level of THs concentration is regulated by the hypothalamus-pituitary-thyroid (HPT) axis, that determines the set point of TH production. Hypothalamic thyrotropin-releasing hormone (TRH) stimulates the synthesis and secretion of pituitary thyrotropin (thyroid-stimulating hormone, TSH), which acts at the thyroid to stimulate all steps of THs biosynthesis and secretion. In turn, the THs control the secretion of TRH and TSH by negative feedback to maintain physiological levels of the main hormones of the HPT axis.

Due to their insoluble nature, more than 90% of total THs released by the thyroid are reversibly bound to plasmatic proteins, such as thyroxine-binding globulin (TBG), transthyretin (TTR, previously known as T4-binding prealbumin) or serum albumin, that maintain the bioavailability of THs and increase the half-life of both T3 and T4 (6,7).

Only a small percentage of the THs are free, around 0.04% for T4 (fT4) and 0.4% for T3 (fT3). Additionally, the bound and free thyroid hormones are in constant equilibrium and it is assumed that to enter the cells, T3 must be in the free form.

Although T4 is produced by the thyroid gland, the major quote of T3 originates from the extra-thyroidal metabolism of T4 into T3. In fact, while around 20% of T3 is directly secreted by the thyroid gland, the residual percentage of T3 is derived from outer ring deiodination of T4 in peripheral tissues, through a potent mechanism of pre-receptor control of TH action at cellular level. This reaction, called 5′-deiodination, is catalyzed by two selenoproteins, the type 1 or type 2 iodothyronine deiodinase (D1 or D2), which act as TH-activating enzymes.

T4 can also be metabolized by conversion to reverse T3 (rT3), which is an inactive metabolite due to its nearly complete inability to bind the thyroid hormone nuclear receptors. rT3 is generated by the removal of the inner ring (5) iodine from T4, through an inactivation step catalyzed mostly by the type 3 iodothyronine deiodinase (D3), which acts as TH-inactivating enzyme.

To exert its functions at cellular level, the TH access to the intracellular compartment is mediated by four different families of TH-transporting proteins, that have been shown to be involved in the traffic of iodothyronines across the cell membrane, with different

patterns of tissue expression (8-11); they are monocarboxylate transporter 8 (MCT8), monocarboxylate transporter 10 (MCT10), transporters of organic anions (OATPs), and L-amino acid transporters (LATS) (12,13). MCT8 is probably the most relevant transporter that transports both T4 and T3 and is expressed in liver, muscle, kidney and in many brain areas (14-16). MCT10, instead, preferentially transports T3 and is expressed in kidney, liver and muscle (11).

Once transported inside cells, the THs levels can be regulated by the activity of deiodinases, that are responsible, in part, for the regulation of intracellular TH action because they can activate (types 1 and 2) or inactivate (types 1 and 3) THs depending on the type of deiodinase expressed and how active the enzyme is in each tissue.

The selenodeiodinases are membrane-anchored proteins of 29-33 kDa that share substantial sequence homology, catalytic properties and contain the selenocysteine (Sec) aminoacid as the key residue within their catalytic center. All the three deiodinases are homodimers whose dimerization is required for full catalytic activity (17,18). The unique feature of selenoproteins in general, and deiodinases in particular, lies in the recoding of the UGA codon from a stop codon to Sec-insertion codon by the presence of the SECIS element in the 3′-UTR of the respective mRNAs. Iodinated contrast agents such as iopanoic acid inhibit all three deiodinases, while propylthiouracil is a relatively specific inhibitor for DIO1.

Type 1 iodothyronine deiodinase (D1) is localized in the plasma membrane and is present in almost all human cells, but the highest concentrations were found in the thyroid, liver and kidneys (19). D1 is able to exert both activating and inactivating functions.

Type 2 iodothyronine deiodinase (D2) is localized in the endoplasmic reticulum (ER), with a half-life of ~ 45 minutes. Its relatively short half-life is due to ubiquitination and proteasome uptake, a feature that is accelerated by interaction with its natural substrate, T4 (20). D2 is expressed in thyroid, skeletal muscle, brown adipose tissue and brain (19), where it is essential for providing the appropriate levels of T3 during the critical period of development of the central nervous system. Responsible for the specific deiodination of T4 into T3, D2 enzyme is considerably more efficient than D1 in the removal of an outer ring iodine atom from the pro-hormone T4 to generate the physiologically active product T3 (21,22).

Type 3 iodothyronine deiodinase (D3) is localized in the plasma membrane and is highly expressed in pregnant uterus, placenta, fetal and neonatal tissues, playing an important role during embryonic development protecting the fetus from excessive exposure to active thyroid hormone. It is also expressed in the brain and skin, but in adult healthy tissues expression levels are very low (23). Recent studies have revealed reactivation of D3 expression in specific pathophysiological contexts correlated with hyperproliferation conditions as cancer.

Inside the cells, the effects of THs are mediated mostly by genetic alterations mainly through the T3 binding to thyroid hormone receptors (THRs, TRα and TRβ, which are encoded by THRA1, THRB1, and THRB2 genes, respectively) (24,25), a family of ligand-dependent transcription factors that modify gene expression by enhancing or inhibiting the expression of target genes by binding to specific DNA sequences, known as TH response elements (TREs). T3 is the preferred ligand of THRs therefore, since the serum concentration of T4 is 100-fold higher than that of T3, this undergoes extra-thyroidal conversion to T3. The importance of T3 generation is that the affinity of THRs for T4 is 10-fold lower than that for T3, and thus the conversion activates T4.

2.2 The relationship between thyroid hormone and skin

The skin, the outermost layer of the body with a very extensive surface area, provides the first line of defence against microbial pathogens and contributes to barrier immunity against external physical or chemical insults. The skin also has important homeostatic functions such as reducing water loss and contributing to thermoregulation of the body.

In mammals, epidermal development is a multistage process consisting of epidermal specification, commitment, stratification and terminal differentiation, as well as morphogenesis of its derivatives. To accomplish these feats, the epidermis constantly replenishes itself, thanks to the presence of stem cells that are capable of self-renewal and of producing transiently amplifying progenitor cells (26).

The skin consists of three layers, in order epidermis, dermis and subcutaneous layer. The epidermis is the top layer of the skin and consists of a thin layer of stratified squamous epithelium, composed of different strata of keratinocytes in progressive stages of differentiation, as well as melanocytes, which provide a barrier from ultraviolet (UV) radiation through expression of melanin. From deep to superficial, the epidermis is organized in five layers, that are the stratum basale, stratum spinosum, stratum

granulosum, stratum lucidum and stratum corneum. The stratum basale is the bottom layer and is responsible for the constantly renewing of the epidermal cells, through an epidermal stem cell compartment residing non only in the basal layer of the epidermis but also in a specific region of the outer root sheath, named *bulge*. This layer contains just one row of undifferentiated epidermal cells, known as basal keratinocytes, that express basal keratins K5 and K14 and divide frequently to replenish the basal layer (27,28). Basal keratinocytes that move into the stratum spinosum differentiate, changing from being columnar to polygonal in shape and begin the synthesis of keratins that are distinct from the basal-layer keratins and release a water-repelling glycolipid that helps prevent water loss from the body, making the skin relatively waterproof. Under physiological conditions, as cells exit from the basal layer and begin their journey towards the skin surface, they switch from the expression of keratins K5/K14 to K1/K10 (27,28). As new keratinocytes are produced at the top the stratum basale, the keratinocytes of the stratum spinosum are pushed into the stratum granulosum, consisting of three to five layers deep of cells that become flatter and generate large amounts of the proteins keratin and keratohyalin, that make up the bulk of the keratinocyte mass in the stratum granulosum and give the layer its grainy appearance. The stratum lucidum is a smooth, seemingly translucent layer of the epidermis located just above the stratum granulosum and below the stratum corneum. The keratinocytes that compose the stratum lucidum are flattened and densely packed with eleiden, a clear protein rich in lipids, derived from keratohyalin, which gives these cells their transparent appearance and provides a barrier to water. The stratum corneum, as the ultimate product of maturing keratinocytes, is so called due to increased keratinization (or cornification) of the cells in this layer. This dry layer helps prevent the penetration of microbes and the dehydration of underlying tissues and provides a mechanical protection against abrasion for the more delicate, underlying layers. Cells in this layer, known as corneocytes, are shed periodically and are replaced by cells pushed up from the stratum granulosum or lucidum.

The dermis, the second thicker layer, has a relatively low cell volume compared with the epidermis and predominantly consists of the extracellular matrix, such as collagen, and contains structures such as blood vessels, lymphatics, nerves, sweat glands and pilosebaceous units. The deepest layer of the skin is the subcutaneous layer, which consists of subcutaneous fat and connective tissue.

The thyroid-skin connection has become a hot frontier in dermatoendocrinology (29-31). In this context, the pituitary hormone that controls thyroid hormone production, thyrotropin (TSH), caught the attention of skin researchers only after it was reported that the receptor for TSH (TSH-R) is transcribed and translated by selected cultured human skin cell populations and in normal human scalp skin in situ, introducing skin as a non-conventional, peripheral target organ for regulation by TSH (32-34).

The importance of hormonal regulation in the skin is illustrated by the existence of numerous endocrine abnormalities that are associated with disorders of the epidermal barrier, skin pigmentation, and the growth or and development of hairs. Human skin and its appendages are known to express thyroid hormone receptors, TRα and TRβ (35-37), and THs are known to alter either positively or negatively the expression of selected keratins in different pathophysiological conditions (38-42).

Clinical evidence as well as studies in hypothyroid mice models (43-45) also suggest that THs could be involved in epidermal proliferation and differentiation, hair growth, and wound healing besides affecting the function of dermal fibroblasts (46,47). Indeed, TH action is crucial for the balance between proliferation and differentiation in normal and pathological conditions, including epidermal regeneration (44) and cutaneous cancer (1). Keratin genes are known to be affected by triiodothyronine (T3), and this regulation is critical during development. The endocrine controls of keratin expression/synthesis through the modulation of keratinocyte proliferation and differentiation, activates distinct programs for the coordinated expression of proliferation/differentiation-related keratins (42). Hypothyroid states result in poorer wound healing, suggesting a therapeutic role for TH in wound healing, mediated in part by affecting the keratins taking part in epidermal cell proliferation (43,44,48). Hyperthyroidism in humans leads to alterations in the skin homeostasis and increases perspiration, heat, pruritus, itching, urticaria, vitiligo, and enhanced pigmentation. In addition, the epidermis is usually thinner than normal. In hypothyroid subjects, the skin is dry, cold, and rough. The epidermis is hyperkeratotic, alopecia may develop, and there is diffuse myxedema (49).

The concept that a finely tuned TH concentration is essential in the control of proliferation versus differentiation raises the possibility of interfering with such mechanisms for therapeutic purposes.

2.3 Keratinocyte Carcinomas (KCs)

Keratinocyte carcinoma (KC), comprised of cutaneous squamous cell carcinoma (cSCC) and basal cell carcinoma (BCC), are the most frequently diagnosed cancers in the Western world (50,51). Although the exact worldwide incidence of KC is unknown, KC represents a significant health burden in many countries. cSCC comprise about 20% of KC diagnoses. An estimated 3-7% of patients develop metastasis, of whom more than 70% will die from disease (52,53). BCC comprises about 80% of all KC. Despite population studies indicating that the BCC-associated mortality rate is negligible (54), BCC can in rare cases metastasize and lead to death (55).

KC also show a high mutational burden, far exceeding that of other cancers, although the genes mutated vary between BCCs and cSCCs (56-59). Exome sequencing of cSCC shows highest levels of TP53 mutations and loss of function CDKN2A mutations. Commonly mutated genes in BCC include those in the sonic hedgehog (SHH) signaling pathway (PTCH1, SUFU, SMO) as well as TP53 (60).

Several treatment methods are available to treat KC. Surgery and/or chemotherapy remain the mainstay of treatment for invasive KC, instead non-surgical destructive options, that include cryosurgery, electrodessication and curettage (EDC), are indicated for low-risk primary KCs (61). Since delaying detection or treatment of KC can have serious consequences and metastatic SCCs are correlated with an extremely poor long-term prognosis (62), to develop better clinical treatments and chemoprevention strategies for SCC, there is a need to achieve a better understanding of the biology of the disease through the development of animal models that recapitulate human cSCC, crucial for understanding the molecular pathogenesis of these tumors.

SCC development through the canonical carcinogenesis model in mice comprises a multistep progression process starting from the precancerous actinic keratosis (AK) in which keratinocyte atypia is confined to only a portion of the epidermis leading to abnormal differentiation and stratum corneum thickening with retained nuclei. When keratinocyte atypia progresses to include the entire epidermis, the lesion is defined as SCC in situ (SCCis) (63). Mouse models of SCC tumor formation through chemical carcinogenesis resemble human skin cancers and offer an ideal model to study cancer initiation and growth (64). The most extensively used mouse cancer model is the multi-stage chemically induced skin tumours (65), which represents one of the best-established

in vivo models for the study of the sequential and stepwise development of tumors. In addition, this model can be used to evaluate both novel skin cancer prevention strategies, and the impact of genetic background and genetic manipulation on tumor initiation, promotion and progression.

In the first step of multi-stage chemical carcinogenesis (initiation), mice are treated with a low dose of the mutagen 9,10-dimethyl-1,2-benzanthracene (DMBA). In the second step (promotion), mice are treated with 12-O-tetradecanoyl phorbol-13-acetate (TPA), a drug that stimulates epidermal proliferation. During promotion, benign tumors, defined papillomas, arise, probably as a consequence of additional mutations, some of which will progress into invasive SCC. Interestingly, papillomas often contain activating mutations in *H-Ras* gene, suggesting that this mutation confers a selective advantage to epithelial cells (66). However, not all papillomas contain mutations in the *H-Ras* gene, and some papillomas and SCC in both mouse and human present mutations in the *K-Ras* gene instead (67,68). Whereas Ras mutations seem to be an early step in skin cancer initiation, p53 mutations are associated with malignant progression (64,69). Transcriptional profiling of the different tumor cell populations arising in SCCs presenting EMT revealed that some markers traditionally used to define epithelial state such as Cdh1 or EPCAM were lost in the early step of EMT, while others such as Krt14, Krt5, or Krt8 were completely lost in the late stages of EMT (70). Similarly, mesenchymal markers exhibited different patterns of expression: some known EMT genes and TFs, such as Cdh2, Vim, Snai1, Twist1/2, and Zeb1/2 were highly upregulated in early hybrid states and were maintained at the same level in the more mesenchymal populations, while the expression of Cdh11, Pdgfra, Pdgfrb, Fap, Loxl1, Col24a1, Mmp19, or Prrx1 increased in late stages of EMT. EMT has been also associated with tumor stemness by their increased tumor propagating potential following their transplantation into immunodeficient mice. Forced expression of TFs that promote EMT such as Twist1 or Snail1 in mammary epithelial cells increase their ability to give rise to secondary tumors upon transplantation (71,72).

Although transgenic mice are a strong in vivo model for studying cSCC formation, the inherent differences in skin structure between mice and humans limits direct correlation of murine models with human disease.

2.4 Stem cells in skin cancer

The remarkable regenerative capacity of skin is related to several different kinds of stem cells (SCs) that, as in many other adult tissues, are responsible for tissue homeostasis and regeneration (73,74). Epithelial skin stem cells (ESSCs) are thought to reside in a specialized area of the hair follicle called bulge. Cells in this compartment possess the ability to differentiate into different cell lineages to regenerate not only the hair follicle but also the sebaceous gland and the epidermis. However, more recent studies presented compelling evidence for the existence of independent IFE (interfollicular epidermis) stem cells, as well as for isthmus stem cells, sebaceous gland stem cells and other epidermal progenitors (75).

Unlike epidermal keratinocytes, which are committed to undergo terminal differentiation, skin stem cells have a long-life span and this result in an ability to accumulate multiple genetic mutations that are necessary to induce cancer formation (76). When stem cells possess the ability to originate tumors they are called cancer stem cells (CSCs) (77). These tumor-initiating cells (TICs) are defined as a subpopulation of cancer cells with self-renewing capacity that possess high tumorigenic potential and can undergo multilineage differentiation to give rise to all types of cells present within the malignancies (78).

Many experimental evidence supports the essential role of CSCs in initiation and progression of several range of solid tumors (79). In solid tumors only a fraction of cancer cells present the capacity to reform secondary tumors following their transplantation into immunodeficient mice (80) and different solid tumors, including pancreatic cancer (81), squamous cell carcinomas (SCCs) (82), colon cancer (83), and melanoma (84), have been shown to contain subpopulations of tumor cells with greater ability to propagate the tumors in xenotransplantation assays. Recently, it was demonstrated that CD34-expressing tumor propagating cells (TPCs) with increased clonogenic potential and the ability to form secondary tumors upon transplantation into immune deficient mice have been isolated from DMBA/TPA-induced skin SCC (85).

2.5 Deiodinases and cancer

The first association between THs and malignancies was suggested more than a century ago (86) and, thereafter, more clinical investigations demonstrated that dysthyroidism are associated with tumor formation and progression. Several neoplasias are commonly associated with changes in thyroid state, through modulation of THRs or deiodinases expression (87-90).

How the changes in thyroid state might influence cancer formation was first described in infantile liver hemangiomas (91), a most common tumors of infancy associated with a severe hypothyroidism caused by high levels of type 3 deiodinase activity. Thereafter, also pediatric and adult liver vascular tumors were associated with severe states of hypothyroidism associated with increased expression and activity of D3 (92,93). Several studies based on the molecular mechanisms associated with increased type 3 deiodinase expression demonstrated that D3, which is an oncofetal protein, rarely expressed in adult life, is re-activated in tumorigenic contexts and that its upregulation is induced by the Shh pathway and the MAPK signaling cascade (94,95). Indeed, the anti-tumorigenic action of TH in BCCs can be attributed to its ability to reduce tumor cells proliferation and promote the apoptotic rate (94).

D2 and D3 mRNA transcripts, as well as D2 and D3 activities, are normally present in epidermal keratinocytes, in according with their novel endocrine function in the skin (96,97). Cutaneous BCC is an excellent model to study the effects and the role of THs in epithelial neoplasias, since express high levels of D3 (1-3,98) and moderate levels of D2 (94).

Several studies based on the role of D2 in cancer revealed that D2 expression is much higher in most brain tumors such as astrocytoma and glioblastoma, with the highest D2 activity in gliosarcomas and oligodendrogliomas (99-101). Furthermore, several neoplastic cell lines exhibit high D2 expression as compared with their normal counterparts, such as placenta and JEG3, a choriocarcinoma cell line (102). At the same time, D2, which is expressed in mesothelial cells, has higher expression in the mesothelioma cell line (MSTO-211H), with the highest levels of D2 ever seen in cultured cells (103). The expression of D2 mRNA and the presence of D2 activity were detected also in human osteoblast-like osteosarcoma (SaOS-2) cell line but this time in lower amount compared with the normal human osteoblast (NHOst) cells (104).

2.6 NANOG in cancer stem cells and tumor development

NANOG is a key transcription factor critical for the acquisition and maintenance of both embryonic and induced pluripotency (105,106). In addition to its critical role during embryogenesis (107,108), it has been recently demonstrated that NANOG exerts a lineage-restricted mitogenic function in stratified epithelia in adult tissues (109). Inducible ubiquitous overexpression of NANOG in mice selectively caused hyperplasia in stratified epithelia, as well as increased proliferation and aneuploidy. In addition, NANOG overexpression in mouse skin epithelia was found to favour malignant transformation of skin papillomas induced by chemical carcinogenesis, thus providing an in vivo evidence for the oncogenic role of NANOG in squamous cell carcinomas (110).

Furthermore, NANOG has been found frequently aberrantly expressed in a variety of human cancers, including head and neck squamous cell carcinomas (HNSCC), oral squamous cell carcinoma (OSCC) and cutaneous SCCs (cSCCs), and in early stages of laryngeal carcinoma (110-113). The profound expression of NANOG in cancer cells along with its capacity to promote mesenchymal traits, migration and invasion, and chemoresistance together suggested that NANOG is a central determinant that drives EMT-like programmes in several cancer cell lines (114). Nevertheless, the role of NANOG in the early stages of tumourigenesis and its possible implication in malignant transformation and acquisition of an invasive phenotype remains to be determined.

High levels of NANOG are associated with aggressive tumor phenotypes. In this regard, it would be possible consider the great applicability potential of NANOG expression as an early cancer risk biomarker, suggesting a novel role for NANOG as an early cancer risk marker in patients with precancerous lesions.

3. Aim of the project

A precise regulation of the TH-dependent landscape of gene expression is essential in a vast range of biological processes, both in physiological or in pathological conditions, in particular in tumorigenesis. Dysregulation of the TH axis was shown to affect cancer outcomes (115). Preclinical (116-121) and clinical (122-125) evidences indicate that the hormonal context plays a crucial role in determining cancer outcome and several studies have further shown promising outcomes following chemical reduction of THs. Since endocrinological parameters such as THs modulate proliferative, metabolic, and cancer-associated angiogenic pathways (126), it is surmised that their levels can be associated with cancer development and progression.

The possibility of locally adjust the intracellular THs availability through the dynamic expression of deiodinases might represent a valid therapeutic approach to identify several new candidates for anti-cancer therapy and improve THs-mediated tumor control.

Based on above considerations, my PhD project aimed to expand the use of deiodinases as a tool with which to locally modulate the TH action in different physiopathological contexts, in order to assess the role of TH metabolism not only in a context of relative benign tumorigenesis, as in the case of BCCs that are not prone to progress, but also during the different stages of the neoplastic process of cutaneous SCCs. In detail, we determined the effects of TH signaling and its regulators in neoplastic processes, specifically investigating the functional implication of D2 in KCs and identifying a comprehensive mechanistic insight into the regulation of type 2 deiodinase in skin cancer. The functional interplay between TH and oncogenic pathways is likely to have broad implications, not only for the role of TH action in skin, but also for the identification of novel potential therapeutic and preventative strategies aimed at interfering with this signaling in other pathological contexts and that may be ready for immediate application.

4. Results

4.1 Type 2 deiodinase is dynamically regulated during epithelial tumorigenesis

To investigate the role of TH in epithelial tumorigenesis, we studied the expression of TH-modulating enzymes in different stages of SCC using the two-step chemically induced carcinogenesis model (Figure 1A) (127). To overcome the lack of commercially available functional D2 antibodies, carcinogenesis experiments were performed in D2-FLAG mouse model (128), in which the endogenous *Dio2* gene is fused to the FLAG tag. As shown in Figure 1B, D2 and D3 are dynamically expressed during SCC tumor initiation and progression: while D3 was highly expressed during the initial tumorigenic step and peaked at the hyperplastic epidermis stage up to the formation of papillomas, D2 expression began at later time points and reached a nadir at the final phases of tumorigenesis, when papillomas lose their differentiation potential, become more invasive and turn into SCCs. D2 signal was closely associated with K8, which is a well-differentiated squamous cell carcinoma marker and whose expression is absent in normal epidermis (129). mRNA analysis confirmed the sequential expression of D3 and D2 at 15 and 30 weeks after DMBA/TPA treatment (Figure 1C). Co-expression of D2 and D3 with markers of specific stages of tumorigenesis was confirmed by Western Blot analysis (Figures 1D-E). D2 expression was associated with reduced E-cadherin and enhanced vimentin expression, which is a sign of the EMT typical of advanced SCCs. Thus, our results show that the EMT of SCC coincides with a switch in D3-D2 deiodinases. Indeed, while D3 is a marker of the initial stages of tumorigenesis, D2 expression is associated with cancer progression.

4.2 Sustained TH signaling induces epithelial-to-mesenchymal transition (EMT) and fosters tumor invasion

To gain insight into the role of TH in tumor progression, we disrupted the TH signal balance by depleting D2 in the epidermal compartment. To this end, we crossed the D2-floxed mouse model (2) with the K14-Cre-ERT mouse model (130), in order to generate a strain that may be useful for studying the keratinocyte-specific D2 depletion. To evaluate tumor progression in an epidermal-specific D2KO background (sD2KO), we depleted D2 from the epidermal compartment by administrating tamoxifen before the DMBA/TPA treatment and analyzed the skin lesions 20 weeks later (Figure 2A). As

shown in Figures 2B-C, D2-depletion increased the frequency of hyperplastic lesions and papillomas, and increased the level of K6 in D2KO papillomas, which confirms that lowering the level of T3 by D2-depletion accelerates tumor growth (Figures 2D-E). Notably, the greater tumor growth in D2KO mice was not associated with greater tumor progression and invasive conversion. Indeed, as shown in Figures 2D-E, K8 expression was lower in sD2KO mice than in control mice, which indicates that D2KO papillomas resist progression to SCC. The lower propensity of sD2KO tumors to acquire a more invasive phenotype was confirmed by the higher E-cadherin/N-cadherin ratio in sD2KO tumors (Figures 2D-E). This finding demonstrates that TH attenuation via D2-depletion reduces the EMT, and that, while increasing tumor formation, it slows tumor progression. Given the effects of D2-depletion in SCC progression and invasiveness, these results suggest that TH D2-produced acts as an up-stream regulator of the cell invasion process.

4.3 The NANOG Transcription factor induces type 2 deiodinase expression and regulates the intracellular activation of thyroid hormone in KCs

To investigate the molecular mechanisms that regulate D2 expression in skin tumorigenesis, we analyzed a region of 1.3 kb upstream of the annotated transcription start site of the *Dio2* gene using the MatInspector software (Precigen Bioinformatics, München, Germany). The *in silico* analysis of the KEGG pathway revealed that 56 genes were putative transcription factors that regulate D2 in cancer (Figure 3A) and, among them, a NANOG binding site was present at position −249 to −231 bp, with a matrix similarity of 0.94 (Figure 3B).

To investigate the mechanisms whereby NANOG regulates D2 expression, we ectopically expressed NANOG in a murine BCC cell line, i.e., the G2N2C cell line (131). NANOG induced the expression of D2 mRNA and the activity of the murine *Dio2*-LUC promoter (Figures 3C-D). Importantly, a chromatin immunoprecipitation assay in BCC cells confirmed that NANOG physically binds the *Dio2* promoter (Figure 3E). Moreover, overexpression of NANOG increased the expression of D2 protein measured by immunofluorescence and Western Blot analysis in primary cultures of mouse keratinocytes from a D2-FLAG mouse (Figures 3F-G).

Next, the core motif of NANOG was mutagenized within the Dio2 promoter region, generating a Dio2-responsive promoter mutant for the NANOG binding site, namely, the

Dio2mut-LUC promoter (Figure 4A, C). When we transfected the wild-type and the mutant D2 promoters, we found that mutagenesis of the NANOG binding site strongly reduced the basal Dio2 promoter activity (Figure 4B, left). Moreover, mutation of the NANOG binding site on Dio2 promoter potently reduced the upregulation of D2 induced by ectopic transfection of NANOG (Figure 4B, right). Finally, to further test the role of NANOG in D2 upregulation, we inhibited NANOG in BCC cells by shRNA-mediated NANOG silencing. In accordance with its role as an inducer of D2 expression, NANOG downregulation resulted in a decrease of D2 expression at mRNA and promoter activity levels (Figure 4D-F). Overall, these results indicate that NANOG positively regulates *Dio2* gene expression.

Having established that NANOG regulates D2 expression in BCC cells *in vitro*, we asked whether their expression correlated in genetically induced BCC tumors *in vivo*. To this aim, we used an inducible mouse model that enables the expression of a constitutively active Smoothened (SmoM2) in the adult epidermal compartment (132) and presents BCC-like tumors, i.e., the K14-Cre-ERT/Rosa-SmoM2-YFP/D2-3xFLAG mouse model (133-135) (herein referred to as K14Cre-SMO). In this mouse model BCCs are induced by the activation of the Smo oncogene in the basal cells of the epidermis by tamoxifen administration. We observed that while D2 was expressed at very low levels in normal skin, its expression rapidly increased in the early stages of tumorigenesis (1-2 weeks after tumor induction) and declined thereafter (Figure 5A). Staining with an anti-FLAG antibody confirmed that D2 was specifically expressed in the early stages of BCC formation, i.e., two weeks after tamoxifen-induced Smo expression (Figure 5B). Notably, NANOG expression paralleled D2 expression. Indeed, NANOG was rapidly upregulated during the early steps of BCC initiation and dramatically decreased some weeks later (Figure 5C). Immunofluorescence analysis confirmed the transcriptional profile of D2 and NANOG during BCC tumorigenesis and revealed co-expression of D2 and NANOG very early in tumorigenesis (Figure 5D). The latter results indicate that the NANOG-D2 axis plays a stage-specific role in BCC development, i.e., NANOG and D2 are required for BCC initiation but not for BCC progression.

Since NANOG is a crucial regulator of stemness, we asked if D2/NANOG co-expression targets both the bulk of tumor cells and the cancer stem cell (CSC) population. To this aim, we isolated the CSCs by fluorescence-activated cell sorting from K14Cre-SMO mice

(by isolating the triple-positive, SmoM2-YFP$^+$/α6-integrin$^+$/CD34$^+$ cells) at different time points after tamoxifen administration (Figure 5E). This strategy discriminates among the total population of cancer cells (SmoM2-YFP$^+$/α6-Integrin$^+$ cells), the CSCs (CD34$^+$ cells), and the somatic cells of the bulk of the tumor (CD34$^-$ cells). Intriguingly, in the CSCs (CD34$^+$ cells), D2 and NANOG were expressed at time 0 (normal skin), and their expression drastically decreased upon tumorigenic induction (Figures 5F, H).

On the contrary, the non-CSC population (i.e., CD34$^-$ cells), which constitutes the bulk of the tumor, confirmed a high D2 and NANOG expression level at the early stages of tumorigenesis, one- and two-weeks following tumor induction (Figure 5G). Therefore, we concluded that D2 and NANOG are specifically expressed in the tumor epithelium of BCC and not in the CD34$^+$ population of CSCs and that the expression of D2 and NANOG in CSCs drastically differs from that in the bulk of tumors.

4.4 The NANOG-D2 axis represents a forward loop that drives the cancer cellular phenotype toward the mesenchymal state

To determine whether D2 and NANOG co-expression is BCC-specific or if it is present in other KCs, we used an alternative model of KC, namely, SCCs (Figure 6A). In agreement with our previous finding (4), we observed that D2 expression in SCCs is activated during the late phase of tumorigenesis and peaks during the final phases of SCC tumorigenesis (Figure 6B). Importantly, NANOG expression was also upregulated during the late stages of tumor progression, when papillomas become more invasive and turn into SCCs (Figure 6C).

Since our general hypothesis is that transformation of benign papillomas to invasive SCC is causally linked to D2-mediated T3 activation, we evaluated the correlation of D2 and NANOG expression also in human SCC tumors using the markers of EMT E-cadherin and ZEB-1, a prime transcriptional factor in the EMT cascade (136), and an up-stream regulator of many EMT-related genes (137), and the relative switch from papillomas to SCC. We collected 72 samples of human tumors at different pathologic states and of diverse tumor grade up to cSCC, to assess the clinical significance of D2-NANOG correlation and the TH signal in human SCCs. The tumor stage of each tumor was evaluated by assessing the expression of E-cadherin and ZEB-1 by immunoistochemical assay (n=20) in formalin-fixed paraffin-embedded biopsies of the five stages of the malignant evolution of keratinocytes towards cSCC: normal epidermis, actinic elastosis,

advanced actinic keratosis, well-differentiated cSCC and poorly differentiated SCC (Figure 6D). We then measured the human D2 and NANOG (encoded by the *NANOG1* gene) mRNA expression by Real-Time PCR from the 20 biopsies and found that they were potently overexpressed in cSCC compared to normal epidermis (Figures 6E-F), consistently with their expression during mouse tumor progression. Pearson's correlation analysis revealed a direct significant correlation between D2 and NANOG in each human SCC sample (Figure 6G: D2 versus NANOG R = 0.868, $p = 0.000011$), confirming the close link between D2 and NANOG in human SCC tumors.

Using the X-Tile program (138), we also analyzed previous data from two collections of tumors in which the gene expression signature of SCC was associated to the risk of relapse, recurrence-free survival and overall survival of patients (139,140).

Kaplan-Meier plots from both data sets showed a striking significant correlation between high D2 levels and risk of relapse, and an inverse correlation with the percent survival of patients (Figures 6H-I). Taken together, the above results suggest that D2 levels are correlated with a more advanced tumor stage and with a poorer prognosis of human cancers, which suggests that D2 is critical in triggering invasiveness and metastatic spreading of SCCs.

5. Discussion

Tumor plasticity is a key variable in the response to therapeutic intervention. Although the classical view of the natural history of cancer is that tumor progression is a linear process and that metastases appear in the late stages of carcinogenesis, many clinical studies show that invasiveness can be acquired at an early stage, and result in metastasis from early neoplasms (141,142). In this project, we demonstrated that D2-produced T3 promotes invasiveness and metastatic conversion of SCC cells in both mouse and human tumors. These data show that in SCC, D2-produced T3 enhances tumor progression, while D2 inhibition reduces the metastatic potential of SCCs. The molecular mode of T3-mediated invasiveness primarily involves the transcription of the master regulator of EMT, ZEB-1, and the induction of the downstream genes for vimentin, N-cadherin, and several metalloproteases (4). However, while the molecular mechanism that controls D3 regulation in cancer is rather known (1-3), the regulation of D2 has not yet been addressed.

It was recently reported that NANOG is frequently aberrantly expressed in squamous cell carcinomas and, in addition, evidence was also provided to support that NANOG plays an active role *in vivo*, promoting malignant conversion of skin papillomas into carcinomas in transgenic mice (110,143). To further and significantly extend these data, this project investigates for the first time the NANOG/D2 axis not only in early stages of KCs tumourigenesis, but also in the late stages to uncover its role in malignant transformation and potential clinical application as cancer risk marker. We describe a novel regulation loop in which NANOG positively regulates the D2 enzyme and induces the upregulation of thyroid hormone signaling in BCC and SCC cells. In this model, NANOG and D2 play stage-specific roles in KCs. In the relatively benign BCC tumors, the two proteins are expressed only in the early phases of tumorigenesis. In the more aggressive SCC tumors, NANOG and D2 are expressed at the late stages of tumorigenesis, during which they support invasiveness and EMT. Common downstream target genes code for ZEB-1, vimentin, E-cadherin, and metalloproteases, thereby resulting in enhanced cell migration and mesenchymal phenotype.

It is not known whether NANOG expression is restricted to CSCs or whether it is also expressed in the tumoral mass of somatic cells (144). Unexpectedly, our data show that D2 and NANOG are highly expressed in the cells of the tumoral bulk ($CD34^-$ cells), while their expression is extremely low in the stem cell population ($CD34^+$ cells). This finding

suggests that NANOG plays a specific cancer-related role in tumoral cells that is not associated with its ability to induce stemness. Although this finding seems to be in contrast with NANOG as a stem gene, it is in line with the finding that NANOG is expressed in adult stratified epithelia, particularly, in the esophagus, forestomach, skin, urothelium, and mucosal tissue (145), which indicates that this transcriptional factor plays a more complex role in somatic cells than hitherto believed.

A novel finding of our study is that NANOG is a positive regulator of TH signaling. Indeed, by inducing D2 expression, NANOG upregulates the production of the active TH (T3) in the target cells. Our data indicate that in SCC cells, this represents a forward loop that drives the cancer cellular phenotype toward the mesenchymal state (Figure 6J). Thus, one effect of inducing NANOG expression is to activate the T4-to-T3 conversion by D2, thereby activating a downstream EMT axis. This finding is consistent with the finding that D2 and NANOG expression is associated with a worse SCC prognosis (4,110) and may belong to the molecular machinery of tumor progression. However, many steps of this mechanistic model still require experimental explanations. Moreover, it remains unclear at present whether NANOG-D2 regulation is related only to epithelial cancer cells or is effective in controlling TH signaling in many other pathophysiological contexts, but our findings suggest an unprecedented clinical application of NANOG/D2 as biomarkers for cancer risk assessment.

6. Materials and Methods

6.1 Cell cultures and transfections

G2N2C cells were derived from transgenic mice expressing a constitutively active form of Gli2 under the control of the keratin 5 promoter (131) and isolated from trichoblastomas. The latter are BCC-like tumors, and are referred to as BCC cells throughout this article. G2N2C cells were cultured in low-calcium medium, with 8% Ca^{2+}-chelated fetal bovine serum (FBS) and keratinocyte growth factor (KGF, 1.0 ng/mL) (Sigma-Aldrich, St. Louis, MO, USA). Transient transfections were performed using Lipofectamine-2000 (Invitrogen™, Carlsbad, CA, USA), according to the manufacturer's instructions.

6.2 Real-Time PCR

Messenger RNAs were extracted with TRIzol reagent (Invitrogen™). Complementary DNAs were prepared with SuperScript™ VILO™ MasterMix (Invitrogen™) as indicated by the manufacturer. The cDNAs were amplified by PCR in a CFX Connect Real-Time PCR Detection System (BioRad, Hercules, California, USA) with the fluorescent double-stranded DNA-binding dye SYBR Green (BioRad). Specific primers for each gene were designed to work under the same cycling conditions (95°C for 10 min followed by 40 cycles at 95°C for 15 s and 60°C for 1 min), thereby generating products of comparable sizes (about 200 bp for each amplification). Primer combinations were positioned whenever possible to span an exon-exon junction and the RNA digested with DNAse to avoid genomic DNA interference. Primer sequences are indicated in the Table 1. For each reaction, standard curves for reference genes were constructed based on six four-fold serial dilutions of cDNA. All samples were run in triplicate. The template concentration was calculated from the cycle number when the amount of PCR product passed a threshold established in the exponential phase of the PCR. The relative amounts of gene expression were calculated with Cyclophilin-A expression as an internal standard (calibrator). The results, expressed as N-fold differences in target gene expression, were determined as follows: $N^{*}target = 2^{(\Delta Ct\ sample - \Delta Ct\ calibrator)}$.

6.3 Protein extraction from skin and Western Blot analysis

Dorsal skin was removed from mice and immediately snap-frozen in liquid N_2. 800 µL of Lysis Buffer (0.125 M Tris pH 8.6; 3% SDS, protease inhibitors including PMSF 1.0 mM and phosphatase inhibitors) were added to all dorsal skin samples, which were then

homogenized with TissueLyser II (QIAGEN, Hilden, Germany). Total tissues protein or cell protein was separated by 10% SDS–PAGE followed by Western Blot. The membrane was then blocked with 5% non-fat dry milk in PBS, probed with specific antibodies (listed in Table 2) overnight at 4°C, washed, and incubated with horseradish peroxidase-conjugated anti-mouse immunoglobulin G secondary antibody (1:3000). Anti-Tubulin antibody was used as loading control. Band detection was performed using an ECL kit (Millipore, Burlington, Massachusetts, USA). The gel images were analyzed using ImageJ software (NIH Image, Bethesda, Maryland) and all Western Blot were run in triplicate.

6.4 Analysis of transcription factor binding sites (TFBSs)

We searched the murine *Dio2* promoter for putative Transcription factor binding sites (TFBSs) using MatInspector (ver. 9.1). Binding sites were compared with database, in terms of core and matrix similarity scores 0.90 (maximum 1.00). The position analyses of common TFBSs were performed in Excel. Position analyses of common TFBSs were performed in Excel and reported in Table 3.

6.5 Chromatin immunoprecipitation (ChIP) assay

SCC cells were transfected with p53-FLAG plasmid or a negative control plasmid, i.e. CMV-FLAG, for 48 h. Approximately 2×10^6 cells were fixed for 10 minutes at 37°C by adding 1% formaldehyde in growth medium. The reaction was quenched by the addition of glycine to a final concentration of 0.125 M. Fixed cells were harvested and the pellet was resuspended in 1.0 mL of lysis buffer containing protease inhibitors (200 mM phenylmethylsulfony fluoride (PMSF), 1.0 µg/mL aprotinin). The lysates were sonicated to obtain DNA fragments of 200-1000 bp. Sonicated samples were centrifuged, and the soluble chromatin was diluted 10-fold in dilution buffer and used directly for ChIP assays. An aliquot (1/10) of sheared chromatin was further treated with proteinase K, extracted with phenol/chloroform and precipitated to determine DNA concentration and shearing efficiency (“input DNA”). Briefly, the sheared chromatin was pre-cleared for 2 hours with 1.0 µg of non-immune IgG (Calbiochem, Sigma-Aldrich) and 30 µL of Protein G Plus/Protein A Agarose suspension (Calbiochem, Sigma-Aldrich) saturated with salmon sperm (1.0 mg/mL). Precleared chromatin was divided in aliquots and incubated at 4°C for 16 h with 1.0 µg of anti-FLAG. After five rounds of washing, bound DNA-protein

complexes were eluted by incubation with 1% sodium dodecyl sulfate-0.1 M $NaHCO_3$ elution buffer. Formaldehyde cross-links were reversed by incubation in 200 mM NaCl at 65°C. Samples were extracted twice with phenol-chloroform and precipitated with ethanol. DNA fragments were used for Real-Time PCRs.

6.6 Short Hairpin RNA-Mediated Knock-Down of NANOG

BCC cells were grown in p60 plates until they reached 60% confluence and then transfected with shRNA targeting endogenous NANOG (shNANOG-1 and 2) or a scramble shRNA (shCTR) as a negative control using Lipofectamine-2000 (InvitrogenTM). shRNA-targeted NANOG sequences were selected from the BLOCK-iTTM RNAi Designer (InvitrogenTM, Thermo Fisher Scientific). Oligos were designed and ordered from Eurofins Genomics. shRNA oligos were cloned into the EcoRI and XhoI sites of a pcRNAi plasmid. Forty-eight hours after transfection, total protein lysate was collected and analyzed by Western Blot, and total RNA was extracted and analyzed by Real-Time PCR. The sequences of oligonucleotides used for Real-Time PCR are shown in Table 1. The list of the antibodies used is shown in Table 2.

6.7 Animals, histology and immunostaining

sD2KO (K14-Cre-ER^T-$D2^{fl/fl}$) mice were obtained by crossing the keratinocyte-specific conditional K14-Cre-ERT mouse (130) with D2-floxed mice (2). D2 depletion was induced by treatment with 10.0 mg of tamoxifen at different time points as indicated in each experiment. The generation of D2-3x-Flag is described elsewhere (128). Skin lesions were harvested at different time points after tamoxifen administration and DMBA-TPA treatment.

$K14Cre^{+/-ERT}$/Rosa-SmoM2-YFP/D2-3X-Flag (K14Cre-SMO) mice were obtained by crossing the keratinocyte-specific conditional $K14Cre^{+/-ERT}$/Rosa-SmoM2-YFP mice with the D2-3X-Flag mice. The expression of a constitutively active Smoothened mutant (SmoM2) in the adult epidermal-specific compartment was induced by treatment with 10.0 mg tamoxifen. All animal experiments and mouse husbandry were carried out in the animal facility of CEINGE − Biotecnologie Avanzate, Naples, Italy, in accordance with institutional guidelines (Authorization n. 354/2019-PR by the Ministero della Salute).

For immunofluorescence and histology, ears from a K14Cre-SMO mouse were embedded in paraffin, cut into 7.0 μm sections, and H&E-stained. Slides were baked at 37°C,

deparaffinized by xylene, dehydrated with ethanol, rehydrated in phosphate buffer solution (PBS), and permeabilized by placing them in 0.2% Triton X-100 in PBS. Antigens were retrieved by incubation in 0.1 M citrate buffer (pH 6.0) or 0.5 M Tris buffer (pH 8.0) at 95°C for 5 minutes. Sections were blocked in 1% BSA/0.02% Tween/PBS for 1 hour at room temperature. Primary antibodies were incubated overnight at 4°C in blocking buffer and washed in 0.2% Tween/PBS. Secondary antibodies were incubated at room temperature for 1 hour, and washed in 0.2% Tween/PBS. Images were acquired with a Leica DMi8 microscope and the Leica Application Suite LAS X Imaging Software.

6.8 DMBA/TPA carcinogenesis

The dorsal skin of 2 months old mice was treated with a single dose (100 μL, 1.0 mg/ml) of the carcinogen 7,12-dimethylbenz[a]anthracene (DMBA) resuspended in propanone, followed by multiple applications of the tumor promoter 12-O-tetradecanoylphorbol-13-acetate, TPA (150 μL, 100 μM) in the two-stage protocol. Experiments in D2-floxed mice were performed using 30 CTR mice and 30 sD2KO mice. Experiments in D2-Flag mice were performed using 8 mice. In all the cohorts there were approximately as many females as male mice.

6.9 Isolation of CSCs

Dorsal and tail skins were separated from the dorsal and tail bone and incubated overnight in 0.25X trypsin at 4°C. The next day the epidermis was separated from the dermis and incubated for 15 minutes in 0.25X trypsin. Trypsinization was neutralized by adding DMEM containing 10% FBS. The cell suspension was then passed twice through a 70.0μm cell-strainer. Isolated keratinocytes were immunostained with APC anti-mouse CD34 Antibody (code 119310, BioLegend, San Diego, CA, USA) and PE Rat Anti-Human α6-integrin (CD49f; code 555736, BD Pharmingen™) by incubation for 45 minutes at room temperature. Fluorescence-activated cell sorting analysis was performed using FACS Canto2 software (FACS Canto2, Becton Dickinson). Live SmoM2-expressing epidermal cells were gated by forward scatter, by side by expression of SmoM2-YFP. For RNA analysis, sorted cells were harvested directly into TRIzol reagent (Invitrogen™).

6.10 Patients and human tissue samples

Formalin-fixed, paraffin-embedded tissue blocks of 72 cutaneous squamous cell carcinomas (cSCCs), diagnosed and excised from May 1993 to May 2018, were retrieved from the archives of the Pathology Section of the Department of Advanced Biomedical Sciences, "Federico II" University of Naples. Out of 72 cases, 50 males and 22 females, the age at diagnosis ranged between 36 and 95 years (mean age 76, median 77). Tumor staging (T1 to T4) according to the 8th AJCC classification was registered only for cSCCs located on head and neck skin and lip. cSCCs developing on mucosal surfaces and less than 1 cm in size were not included in this study. The clinical data and pathological features of the tumors are reported in Table 4. The study design and procedures involving tissue samples collection and handling were performed according to the Declaration of Helsinki, in agreement with the current Italian law, and to the Institutional Ethical Committee guidelines. For immunohistochemistry of human samples, we selected a block of fixed tissue in each case, and one section of the block was stained with hematoxylin/eosin to verify the initial diagnosis; the other sections were used for immunohistochemical investigations. Immunohistochemical analysis was performed on 4-μm thick serial sections mounted on poly-L-lysine-coated glass slides. The sections were deparaffinized and subjected to antigen retrieval by microwave oven treatment (3 min x 4 times, in citrate buffer, pH 6); the backdrop (for blocking non-specific background staining) was removed using the universal blocking serum (Dako Diagnostics) for 15 min at room temperature. Endogenous alkaline phosphatase activity was quenched by adding levamisole to buffer AP (substrate buffer); the slides were rinsed with TRIS+Tween20 pH 7.4 buffer, and incubated in a humidified chamber with primary antibodies anti-E-cadherin (mouse monoclonal antibody, diluted 1:300 1 h at room temperature, BD Biosciences), anti-ZEB- 1 (rabbit polyclonal antibody, diluted 1:200 1 h at room temperature, NBP1-05987 Novus Biologicals, UK) and anti-D3. Then used a biotinylated secondary antibody and streptavidin conjugated with alkaline phosphatase. The reaction was visualized with chromogen fast red, which showed the presence of the antigen that we sought in red (Dako REAL Detection System, Alkaline Phosphatase/RED, Rabbit/Mouse). After weak nuclear counterstaining with hematoxylin, the sections were mounted with a synthetic medium (Entellan, Merck). Positivity for E-

cadherin and ZEB-1 was visualized as red nuclear staining and red membranous staining, respectively. The level of immunostaining was scored semiquantitatively.

6.11 Statistical analyses

All results are reported as means ± SD. Differences between samples were assessed with the Student's two-tailed t test for independent samples. Relative mRNA levels (in which the control sample was arbitrarily set as 1) are reported as results of Real-Time PCR in which the expression of Cyclophilin A served as housekeeping gene. In all experiments, differences were considered significant when p was less than 0.05. Asterisks indicate significance at *$p<0.05$, ** $p<0.01$, and *** $p< 0.001$ throughout.

7. Figures and tables

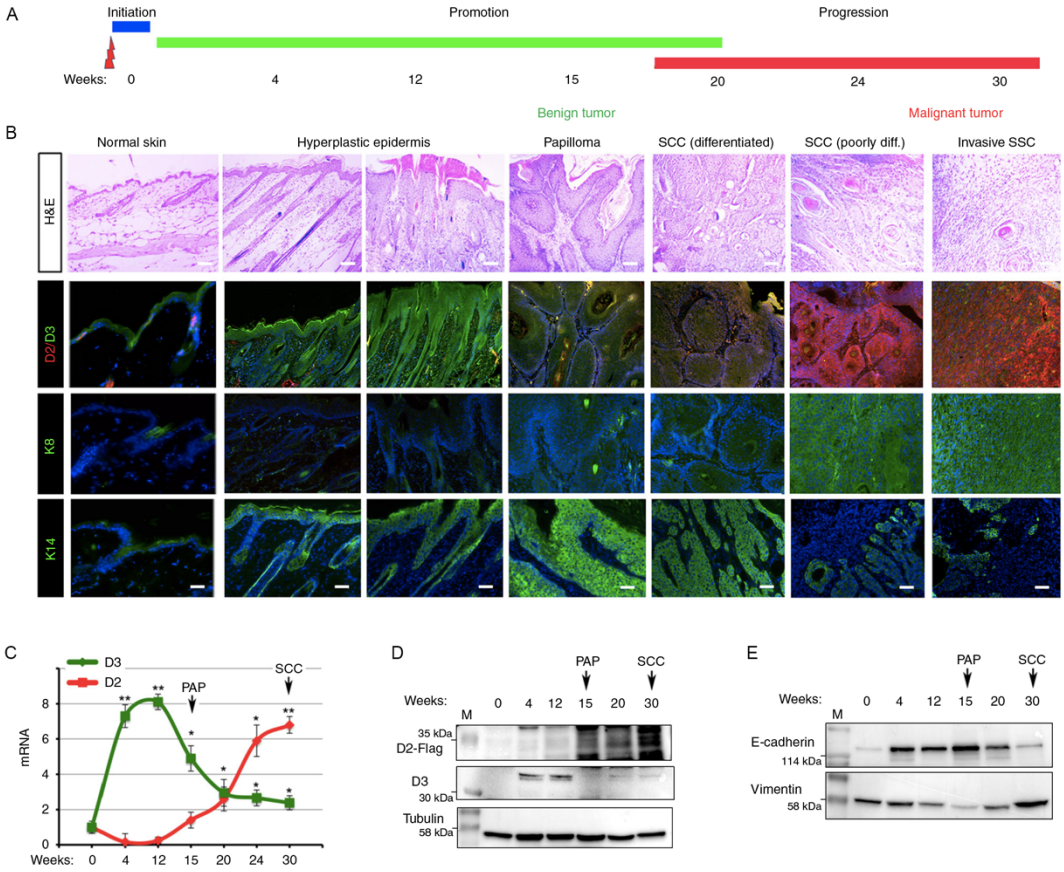

7.1 Figure 1. D2 and D3 are dynamically expressed during SCC tumor initiation and progression. (A) Schematic representation of the two-step carcinogenesis experiment. **(B)** Representative H&E, D2/D3 co-staining, and K8 and K14 staining of DMBA-TPA-treated skins for the indicated weeks. Images represent tumors of one of eight different D2-Flag mice analyzed for each time point ($n = 8$). Scale bar represents 200 µm. **(C)** mRNA levels of D2 and D3 were measured in progressive DMBA-TPA-treated skins as indicated in a and b, by Real-Time PCR analysis (n = 8). **(D)** Western Blot analysis of D2-Flag and D3 expression from skin lesions of D2-3x-Flag mice treated with DMBA-TPA for the indicated times (n = 8). **(E)** Western Blot analysis of E-cadherin, vimentin in the same samples as in (D).

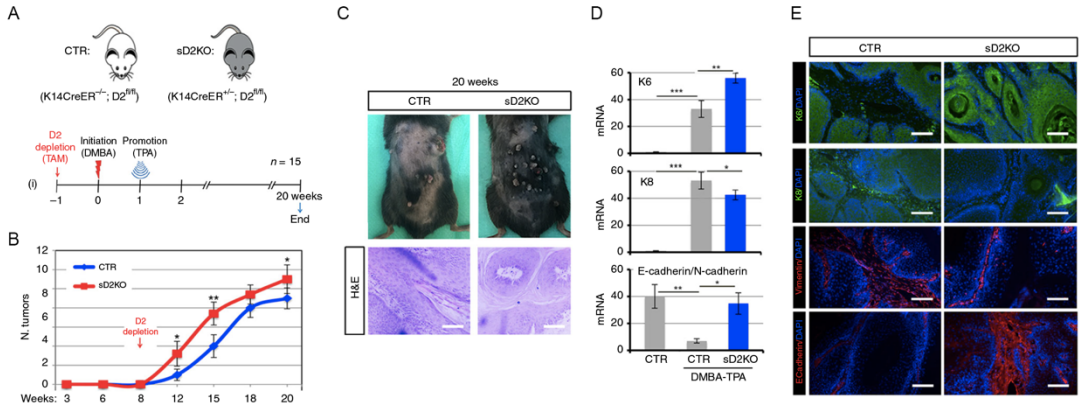

7.2 Figure 2. Attenuation of TH signaling in D2KO mice enhanced tumor growth and reduced the EMT. (A) Schematic representation of D2-depletion and the two-step carcinogenesis experiment in 15 CTR and 15 sD2KO samples (n = 15). **(B)** The number of skin lesions counted during DMBA/TPA treatment in sD2KO and CTR mice. **(C)** Picture of the dorsal skin from CTR (n = 15) and sD2KO (n = 15) mice treated with DMBA/TPA for 20 weeks showing papillomas and advanced SCC (top). H&E of the skin lesions from CTR (n = 8) and sD2KO (n = 12) mice (bottom). Scale bars represent 200 µm. **(D)** The mRNA levels of K6, K8, and E-cadherin/N-cadherin ratio in skin lesions of CTR (n = 15) and sD2KO (n = 15) mice measured by Real-Time PCR analysis. **(E)** Immunostaining for K6, K8, vimentin, and E-cadherin was performed on paraffin-embedded sections of dorsal skin lesions (n = 10 for both groups). Scale bars represent 200 µm.

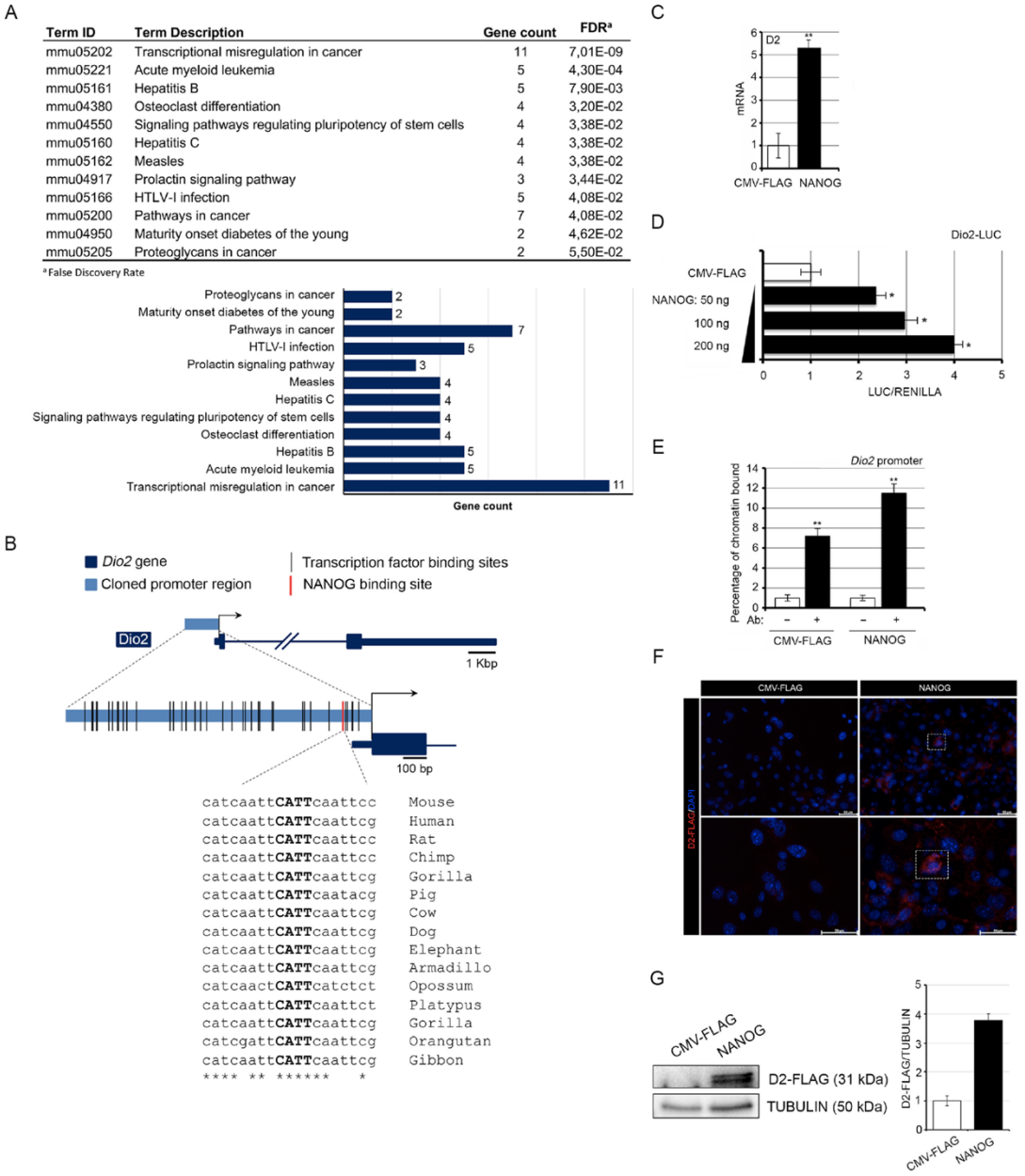

7.3 Figure 3. NANOG positively regulates type 2 deiodinase (D2) transcription. (A) KEGG pathway clusters generated by the *in silico* analysis of the Dio2 promoter region. **(B)** Schematic localization of transcription factors and of the NANOG binding site within the Dio2 promoter region; conservation and Logo representation of the NANOG binding motif. **(C)** D2 mRNA expression was measured by Real-Time PCR in basal cell carcinoma (BCC) cells transiently transfected with a NANOG-expressing vector or the CMV-FLAG plasmid (control). **(D)** BCC cells were transiently transfected with the Dio2–LUC promoter and with increasing amounts of the NANOG plasmid. Cells were harvested 48 h after transfection and analyzed for luciferase activity. CMV-Renilla was co-transfected as an internal control. The results are shown as means ± SD of the LUC/Renilla ratio from at least three separate experiments, performed in triplicate; * $p < 0.05$, ** $p < 0.01$. **(E)** Chromatin immunoprecipitation assay was performed in BCC cells. Immunoprecipitation of chromatin using the anti-NANOG antibody revealed that the Dio2 gene is a direct target of NANOG. **(F)** D2-FLAG expression levels were measured by immunofluorescence analysis of mouse primary keratinocytes from D2-Flag mice transfected with the NANOG plasmid or the CMV-FLAG plasmid. Magnification 10X and 20X; scale bars represent 50 µm. **(G)** Western Blot analysis of D2 expression in the same cells as in F.

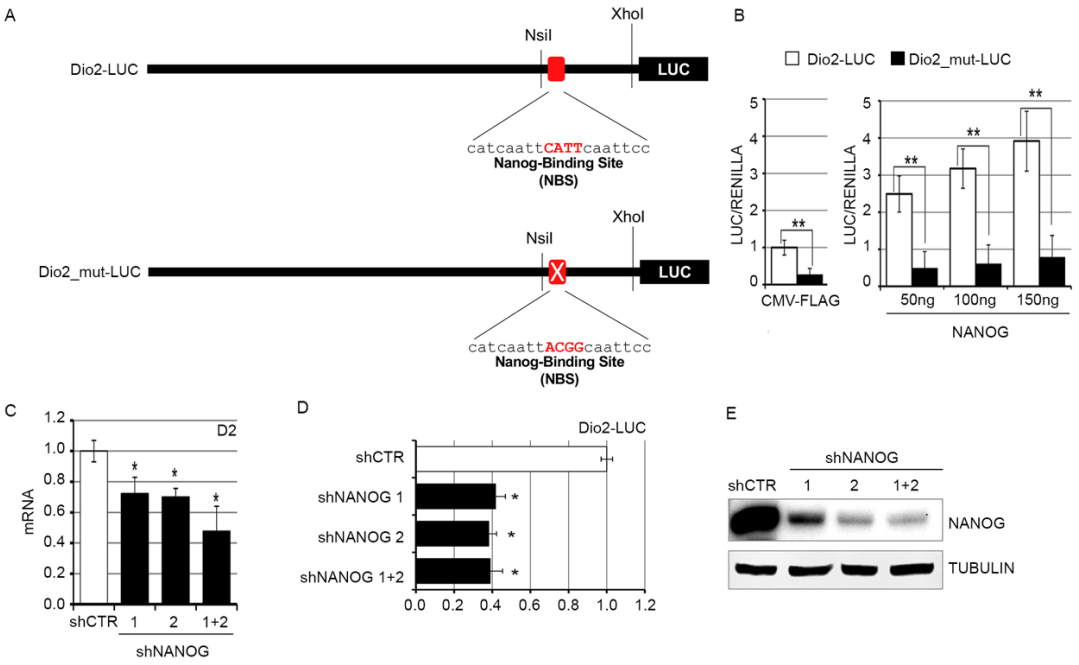

7.4 Figure 5. NANOG downregulation reduces the expression of D2 in BCC cells. (A) Schematic representation of the NANOG binding site mutation within the *Dio2* promoter region. **(B)** BCC cells were transiently transfected with Dio2-LUC promoter or Dio2mut-LUC promoter and CMV-FLAG (left) or increasing amounts of NANOG plasmid (right). Cells were harvested 48 h after transfection and analyzed for luciferase activity. CMV-Renilla was co-transfected as an internal control. The results are shown as means ± SD of the LUC/Renilla ratio from at least three separate experiments, performed in triplicate; * $p < 0.05$, ** $p < 0.01$. **(C)** D2 mRNA expression was measured by real-time PCR in BCC cells transfected with two different NANOG shRNAs, as single plasmids or in combination, or a control (CTR) shRNA as indicated. **(D)** BCC cells were transiently transfected with Dio2-LUC promoter and with NANOG shRNA as in C. Cells were harvested 48 h after transfection and analyzed for luciferase activity. CMV-Renilla was co-transfected as an internal control. The results are shown as means ± SD of the LUC/Renilla ratio from at least three separate experiments, performed in triplicate; * $p < 0.05$, ** $p < 0.01$. **(E)** Validation of effective NANOG down-modulation by two different NANOG shRNA vectors was assessed by Western Blot analysis of NANOG expression in BCC cells.

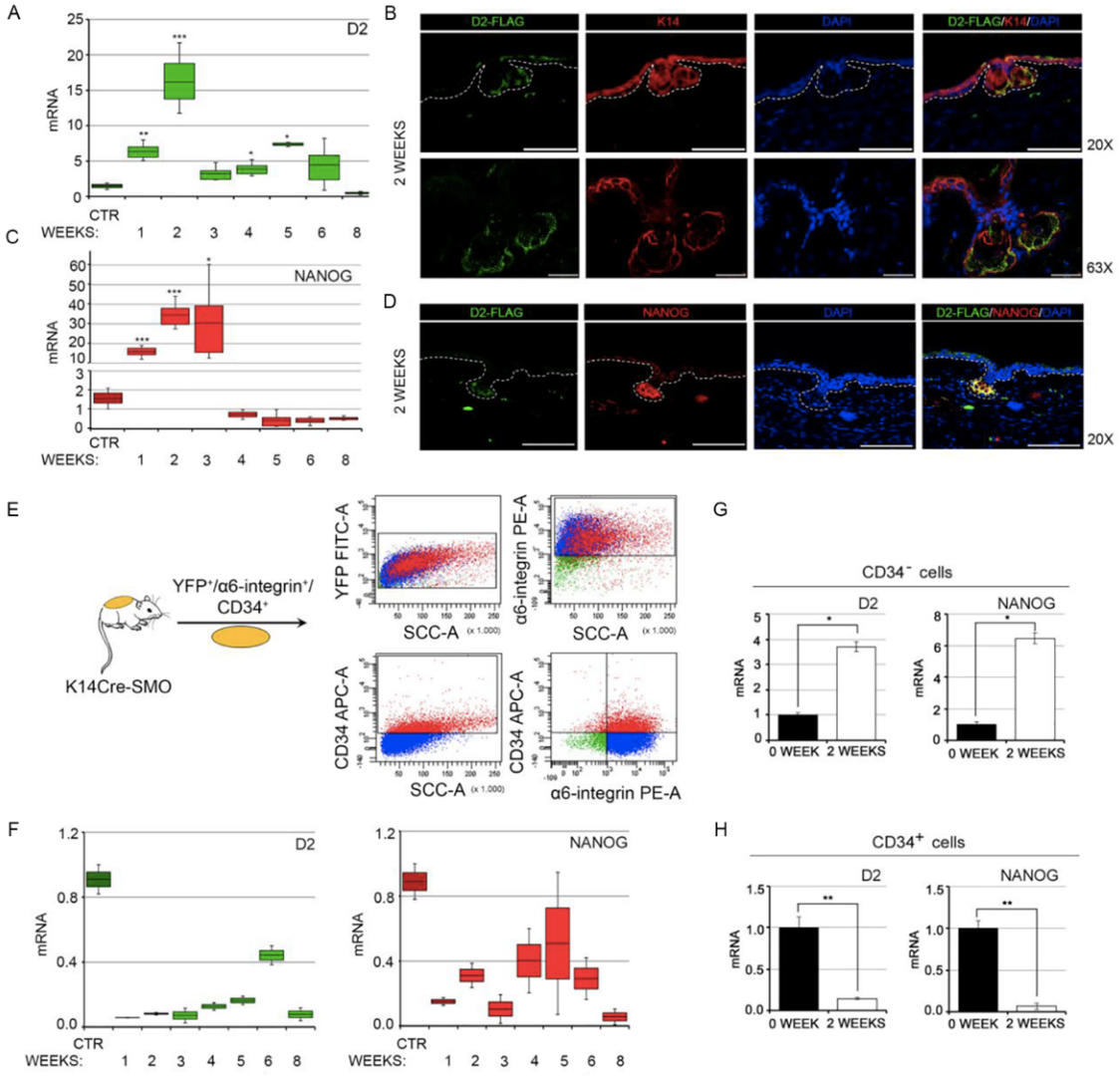

7.5 Figure 5. D2 expression correlates with NANOG expression during BCC tumor formation. (A) D2 expression was assessed by Real-Time PCR at different stages of BCC tumorigenesis in the adult epidermis of K14Cre-SMO mice. (**B**) D2 localization was assessed by immunofluorescence analysis two weeks after the induction of BCC tumorigenesis in the adult epidermis of K14Cre-SMO mice. Magnification 20X and 63X; scale bars represent 100 μm and 25 μm, respectively. (**C**) Relative expression of NANOG mRNA at different stages of BCC tumorigenesis, as in A. (**D**) Representative D2/NANOG co-staining was performed on paraffin-embedded skin sections at two weeks of BCC tumorigenesis from the ear epidermis of K14Cre-SMO mice. Magnification 20X; scale bars represent 100 μm. Data represent the mean of four independent experiments performed in triplicate. (**E**) Schematic representation of the strategy used to isolate cancer stem cell (CSCs) from K14Cre-SMO. (**F**) Transcriptional profile of D2 and NANOG in the CSCs population (CD34+ cells) during BCC tumorigenesis. (**G**) D2 and NANOG mRNA expression levels in FACS-isolated CSCs (CD34+ cells) were measured by Real-Time PCR. (**H**) D2 and NANOG mRNA expression levels in the FACS-isolated non-CSC population (CD34 cells) were measured by Real-Time PCR. Data represent the mean of four independent experiments performed in triplicate; * $p < 0.05$, ** $p < 0.01$, *** $p < 0.001$.

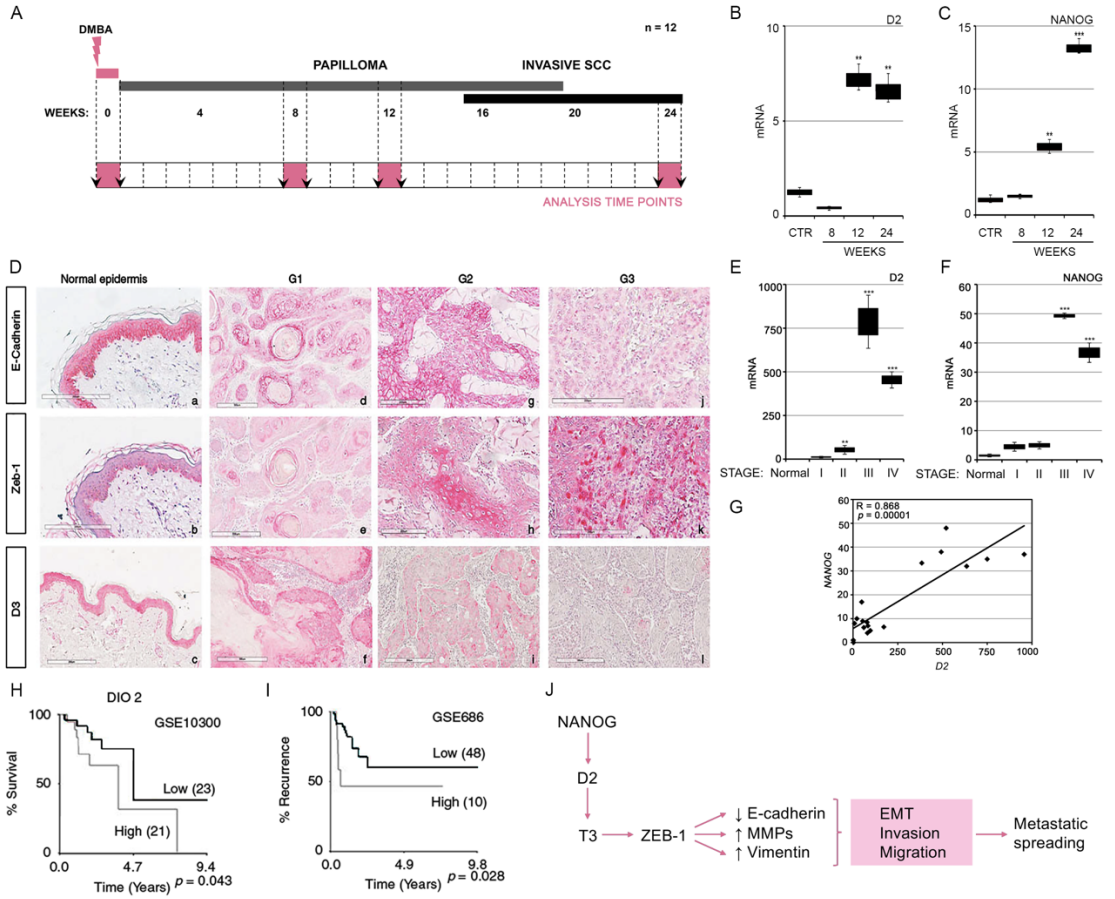

7.6 Figure 6. D2 and NANOG are co-expressed in the late phases of squamous cell carcinoma (SCC) tumor progression. (**A**) Schematic representation of the chemical cancerogenesis experiment for SCC tumor progression in mice. (**B-C**) Expression profile of D2 mRNA and NANOG mRNA during mouse SCC tumorigenesis. Data represent the mean of three independent experiments performed in triplicate. **(D)** Representative images showing immunohistochemical (IHC) staining for ZEB-1, E-cadherin, and D3 proteins in cutaneous squamous cell carcinoma (cSCC). Positive E-cadherin expression (a) and negative ZEB-1 expression (b) in normal tissue, and in G1 cSCC (d, e). Moderate E-cadherin expression (g) and weak ZEB-1 expression (h) in G2 cSCC. Finally, negative E-cadherin expression (j) and positive ZEB-1 expression (k) in G3 cSCC. IHC staining of D3 expression revealed positive D3 expression in normal epidermis (c), a rise in D3 expression in G1 (f) and a drastic decrease of D3 expression at the later stages G2 and G3 (i, l). IHC analysis was performed in 20 different tissues for each grading. **(E-F)** The expression of D2 and NANOG mRNA was measured in human SCC tumors at different pathologic stages in comparison with normal skin counterparts. All samples were runin triplicate and referred to normal skin set arbitrarily as 1. **(G)** Pearson's correlation analysis was performed for the same data as in E-F. PCR analysis was performed in 20 different tissues for each grading. ** $p < 0.01$; *** $p < 0.001$. **(H-I)** Kaplan–Meier plots from two independent data sets (GSE10300 and GSE 686). Black indicates low and gray indicates high D2 expression. The number of tumors in each group is reported in parentheses. **(J)** The NANOG–D2–T3–ZEB-1 axis contributes to the EMT and to the progression to invasive stages of carcinomas.

7.7 Table 1: List of Oligonucleotides

Oligonucleotides used for Real-Time PCR			
GENE	**Name/Gene ID**		
Cyclophilin A	CypA	Forward	CGCCACTGTCGCTTTTCG
		Reverse	AACTTTGTCTGCAAACAGCTC
CYCLOPHILIN A	CYPA	Forward	AGTCCATCTATGGGGAGAAATTTG
		Reverse	GCCTCCACAATATTCATGCCTTC
Dio2	Dio2	Forward	CTTCCTCCTAGATGCCTACAAAC
		Reverse	GGCATAATTGTTACCTGATTCAGG
DIO2	DIO2	Forward	CTCTATGACTCGGTCATTCTGC
		Reverse	TGTCACCTCCTTCTGTACTGG
Dio3	Dio3	Forward	CCGCTCTCTGCTGCTTCAC
		Reverse	CGGATGCACAAGAAATCTAAAAGC
E-cadherin	Cdh1	Forward	CGTCCTGCCAATCCTGATGA
		Reverse	ACCACTGCCCTCGTAATCGAAC
K6	Krt6	Forward	TCGTGACCCTGAAGAAGGATGTA
		Reverse	CCTTGGCTTGCAGTTCAACTT
K8	Krt8	Forward	ACAACAAGTTCGCCTCCTTC
		Reverse	TCTCCATCTCTGTACGCTTGT
N-cadherin	Cdh2	Forward	ACAGTGGAGCTCTACAAAGG
		Reverse	CTGAGATGGGGTTGATAATG
Nanog	Nanog	Forward	AAGAACTCTCCTCCATTCTGAACCT
		Reverse	GCACTTCATCCTTTGGTTTTGAA
NANOG	NANOG	Forward	CTGCTGAGATGCCTCACACG
		Reverse	CTTCCTTTTTTGCGACACTC
Oligonucleotides used for ChIP Analysis			
NANOG-ChIP		Forward	GGTAAACTGGATTAGGGACTGGC
		Reverse	GAGGGAGAAAAGCTAAATTAG

7.8 Table 2: List of Antibodies

Antibodies	**Source**	**Identifier**	**Diluition**
Anti-α-Tubulin antibody, Mouse monoclonal	Sigma-Aldrich	T8203	1:5000 WB
Anti-Cytokeratin 6, Rabbit polyclonal	Covance®	PRB-169P	1:1000 IF
Anti-Cytokeratin 8, Rat monoclonal (TROMA 1)	Hybridoma bank	AB_531826	1:300 IF
Anti-Cytokeratin 14, Rabbit polyclonal	Covance®	CLPRB-155P	1:2000 IF
Anti-D3 (717)	Homemade	Homemade	1:500 WB
Anti-D3 (718)	Homemade	Homemade	1:500 IF 1:500 IHC
Anti-FLAG® M2 antibody, Mouse monoclonal	Sigma-Aldrich	F3165	1:1000 IF 1:1000 WB
Anti-E-cadherin, Mouse monoclonal	BD Biosciences	610181	1:1000 WB
Anti-N-cadherin, Rabbit polyclonal	Elabscience®	E-AB-32170	1:500 WB
Anti-Nanog antibody, Rabbit polyclonal	abcam	ab80892	1:1000 WB
Anti-Vimentin, Rabbit monoclonal	abcam	ab92547	1:2000 WB 1:1000 IF
Anti-ZEB1, Rabbit polyclonal	Novus Bio	NBP1-05987	1:250 IF 1:250 IHC
APC ANTI-MOUSE CD34 ANTIBODY 25 UG	BIOLEGEND	119309	1:100 FACS
PE Rat Anti-Human CD49f Clone GoH3 (RUO)	BD Pharmingen™	555736	1:100 FACS

7.9 Table 3: In silico analysis of Transcription Factor Binding Sites (TFBS) upstream from the Transcription Start Site (TSS) of Dio2 gene

DETAILED MATRIX INFORMATION	START POSITION	END POSITION	ANCHOR POSITION	STRAND	MATRIX SIMILARITY
Nascent polypeptide-associated complex subunit alpha 1	12	0	6	+	0,95
Pre-B-cell leukemia homeobox 3	28	12	20	+	0,957
Hypermethylated in cancer 1 (secondary DNA binding preference)	35	23	29	+	0,957
Cysteine-serine-rich nuclear protein 1 (AXUD1, AXIN1 up-regulated 1)	36	30	33	+	1
SPI-1 proto-oncogene; hematopoietic transcription factor PU.1	50	30	40	+	0,966
Zinc finger protein insulinoma-associated 1 (IA-1) functions as a transcriptional repressor	49	37	43	+	0,949
NMP4 (nuclear matrix protein 4) / CIZ (Cas-interacting zinc finger protein)	61	51	56	+	0,97
CCAAT/enhancer binding protein (C/EBP), epsilon	66	52	59	-	0,993
Polyomavirus enhancer A binding protein 3, ETV4 (Ets variant gene 4)	77	57	67	-	0,95
H6 homeodomain HMX3/Nkx5.1 transcription factor	92	74	83	-	0,921
Myeloid zinc finger protein MZF1	104	94	99	-	1
SPI-1 proto-oncogene; hematopoietic transcription factor PU.1	110	90	100	-	0,965
5' half site of ZTRE motif	112	96	104	+	0,984
Zinc finger and BTB domain containing 7A, pokemon	118	96	107	+	0,941
Kruppel-like zinc finger protein 219	120	98	109	+	0,986
Collagen krox protein (zinc finger protein 67 - zfp67)	118	100	109	-	0,909
Kruppel-like factor 3 (basic)	119	101	110	-	0,99
Myc associated zinc finger protein (MAZ)	116	104	110	-	0,951
GLIS family zinc finger 3, Gli-similar 3	119	103	111	+	0,94
Zinc finger, BED-type containing 4; polyG binding sites	118	104	111	-	0,951
Zinc finger protein insulinoma-associated 1 (IA-1) functions as a transcriptional repressor	117	105	111	-	0,911
Zinc finger transcription factor ZBP-89	123	101	112	+	0,959
3' half site of ZTRE motif	120	104	112	-	0,982
Pleomorphic adenoma gene 1	130	108	119	-	1
Wilms Tumor Suppressor	131	113	122	-	0,951
Homeodomain transcription factor Gsh-2	148	130	139	+	0,966
Photoreceptor conserved element 1	147	131	139	+	0,914
Homeodomain proteins MSX-1 and MSX-2	149	131	140	+	0,989
Evi-1 zinc finger protein, carboxy-terminal zinc finger domain	173	157	165	+	0,909
STAT5: signal transducer and activator of transcription 5	178	160	169	-	0,94
TCF/LEF-1, involved in the Wnt signal transduction pathway	177	161	169	+	0,967
SWI/SNF related, matrix associated, actin dependent regulator of chromatin, subfamily a, member 3	188	178	183	+	0,967
Interferon regulatory factor 3 (IRF-3)	196	172	184	-	0,949
c-Rel	196	182	189	+	0,964
c-Myb, important in hematopoesis, cellular equivalent to avian myoblastosis virus oncogene v-myb	230	210	220	+	0,92
Nuclear factor 1	236	216	226	+	0,91
Liver enriched Cut - Homeodomain transcription factor HNF6 (ONECUT1)	241	225	233	-	0,913
HMG box-containing protein 1	249	227	238	+	0,987
Homeobox transcription factor Nanog	**249**	**231**	**240**	**+**	**0,942**
NMP4 (nuclear matrix protein 4) / CIZ (Cas-interacting zinc finger protein)	266	256	261	+	0,976

Signal transducer and activator of transcription 3	277	259	268	-	0,965
Abd-B-like homeodomain protein Hoxb-9	282	266	274	+	0,914
Transcription factor yin yang 2	286	264	275	+	0,961
Evi-1 zinc finger protein, carboxy-terminal zinc finger domain	285	269	277	-	0,901
Ribonucleoprotein associated zinc finger protein MOK-2 (human)	312	292	302	+	0,992
Regulatory factor X, 5 (influences HLA class II expression)	318	300	309	-	0,981
Fetal Alz-50 clone 1 (FAC1)	321	311	316	-	0,965
Sites bound by FOXP1 and an alternative splicing variant FOXP1_ES, activated in ESCs	325	309	317	-	1
Fetal Alz-50 clone 1 (FAC1)	324	314	319	-	0,97
Sites bound by FOXP1 and an alternative splicing variant FOXP1_ES, activated in ESCs	328	312	320	-	1
Fetal Alz-50 clone 1 (FAC1)	327	317	322	-	0,983
Sites bound by FOXP1 and an alternative splicing variant FOXP1_ES, activated in ESCs	331	315	323	-	1
DRE (dioxin response elements), XRE (xenobiotic response elements) bound by AHR/ARNT heterodimers	349	325	337	-	0,962
Myelin regulatory factor	347	335	341	-	0,958
GTF2I-like repeat 4 of GTF3	355	345	350	+	0,979
Cone-rod homeobox-containing transcription factor	359	343	351	-	0,981
Phox2a (ARIX) and Phox2b	363	343	353	-	0,949
Zinc finger protein insulinoma-associated 1 (IA-1) functions as a transcriptional repressor	368	356	362	+	0,968
TG-interacting factor belonging to TALE class of homeodomain factors	372	356	364	-	1
v-Myb, AMV v-myb	387	367	377	+	0,993
Ets variant 1	397	377	387	-	0,994
Interferon regulatory factor (IRF)-related protein (NF-EM5, PIP, LSIRF, ICSAT)	413	389	401	+	0,974
Signal transducer and activator of transcription 3	416	398	407	-	0,974
Signal transducers and activators of transcription	470	452	461	+	0,914
Hmx3/Nkx5-1 homeodomain transcription factor	471	453	462	-	0,923
Gut-enriched Krueppel-like factor	472	454	463	+	0,976
Hmx3/Nkx5-1 homeodomain transcription factor	476	458	467	+	0,921
Sma- and Mad-related proteins	479	469	474	-	1
Thing1/E47 heterodimer, TH1 bHLH member specific expression in a variety of embryonic tissues	486	466	476	+	0,94
CCAAT/enhancer binding protein beta	505	491	498	+	0,958
Ras-responsive element binding protein 1	540	526	533	+	0,94
Zinc finger protein insulinoma-associated 1 (IA-1) functions as a transcriptional repressor	544	532	538	-	0,921
v-Myb	609	589	599	+	0,97
Forkhead box P1	611	595	603	-	0,985
Androgene receptor binding site, IR3 sites	621	603	612	-	0,982
Myc associated zinc finger protein (MAZ)	627	615	621	+	0,91
Zinc finger protein 263, ZKSCAN12 (zinc finger protein with KRAB and SCAN domains 12)	629	615	622	-	0,949
Zinc finger protein 263, ZKSCAN12 (zinc finger protein with KRAB and SCAN domains 12)	632	618	625	-	0,97
Peroxisome proliferator-activated receptor gamma	666	644	655	+	0,91
Repressive binding sites for glucocorticoid receptor (IR1)	675	661	668	+	0,978
Pleomorphic adenoma gene 1	692	670	681	+	1
3' half site of ZTRE motif	696	680	688	+	0,984
Kruppel-like factor 3 (basic)	699	681	690	+	0,992
Zinc finger, BED-type containing 4; polyG binding sites	697	683	690	+	0,922

MYC-associated zinc finger protein related transcription factor	696	684	690	+	0,901
Collagen krox protein (zinc finger protein 67 - zfp67)	700	682	691	+	0,973
Zinc finger protein 263, ZKSCAN12 (zinc finger protein with KRAB and SCAN domains 12)	698	684	691	-	0,935
Zinc finger and BTB domain containing 7A, pokemon	704	682	693	-	0,949
5' half site of ZTRE motif	704	688	696	-	0,988
c-Rel	709	695	702	-	0,957
GATA-binding factor 2	722	710	716	+	0,905
Zinc finger and BTB domain containing 3	738	728	733	+	0,997
Cysteine-serine-rich nuclear protein 1 (AXUD1, AXIN1 up-regulated 1)	744	738	741	-	1
Calcium-reponse factor	752	742	747	+	0,979
Cellular and viral TATA box elements	787	771	779	+	1
Pit1, GHF-1 pituitary specific pou domain transcription factor	789	775	782	-	0,965
TEA domain family member 4, TEF-3	794	782	788	-	0,942
Distal-less 3 homeodomain transcription factor	805	787	796	-	0,994
Homeobox containing germ cell-specific transcription factor NOBOX	807	789	798	-	0,991
Homeodomain transcription factor Gsh-2	808	790	799	-	0,975
Brain specific homeobox	808	790	799	+	0,974
Photoreceptor conserved element 1	807	791	799	-	0,96
NK1 homeobox 2, Sax1-like	807	791	799	-	0,916
Binding site for S8 type homeodomains	811	791	801	-	0,995
Distal-less homeobox 2	810	792	801	+	0,929
Interferon regulatory factor (IRF)-related protein (NF-EM5, PIP, LSIRF, ICSAT)	827	803	815	-	0,954
Cone-rod homeobox-containing transcription factor / otx-like homeobox gene	835	819	827	-	0,971
CCAAT/enhancer binding protein beta	840	826	833	+	0,945
cAMP-responsive element binding protein	853	833	843	-	0,926
GLI-Krueppel-related transcription factor, regulator of adenovirus E4 promoter	850	838	844	+	0,921
cAMP-responsive element binding protein 1	855	835	845	+	1
cAMP-responsive element binding protein 1	856	836	846	-	1
cAMP-responsive element binding protein	858	838	848	+	0,927
MyT1 zinc finger transcription factor involved in primary neurogenesis	915	903	909	+	0,9
Gut-enriched Krueppel-like factor	928	910	919	-	0,965
Zinc finger with KRAB and SCAN domains 3	937	915	926	+	1
Zinc finger, BED-type containing 4; polyG binding sites	936	922	929	-	0,951
Zinc finger transcription factor ZBP-89	941	919	930	+	0,935
Wilms Tumor Suppressor	941	923	932	-	0,938
Wilms Tumor Suppressor	943	925	934	-	0,961
SRY (sex determining region Y)-box 6	960	938	949	+	0,984
Jumonji, AT rich interactive domain 1B	957	949	953	+	0,961
Muscle TATA box	966	950	958	+	0,901
Gut-enriched Krueppel-like factor	971	953	962	-	0,976
Homeobox and leucine zipper encoding transcription factor	989	975	982	+	0,963
Gut-enriched Krueppel-like factor	1001	983	992	+	0,966
Peroxisome proliferator-activated receptor gamma, DR1 sites	1005	983	994	+	0,913
TG-interacting factor belonging to TALE class of homeodomain factors	1005	989	997	+	1
SWI/SNF related, matrix associated, actin dependent regulator of chromatin, subfamily a, member 3	1036	1026	1031	+	0,986

BARX homeobox 1	1043	1025	1034	-	0,917
Homeodomain transcription factor Gsh-2	1044	1026	1035	-	0,952
Muscle-segment homeobox 1, msh homeobox 1	1044	1026	1035	+	0,907
Special AT-rich sequence-binding protein 1, predominantly expressed in thymocytes, binds to matrix attachment regions (MARs)	1056	1042	1049	-	0,967
Zinc finger protein 652 (ZNF652)	1063	1049	1056	+	0,909
Nuclear factor of activated T-cells	1068	1050	1059	+	0,965
Cone-rod homeobox-containing transcription factor / otx-like homeobox gene	1075	1059	1067	+	0,945
GATA-binding factor 2	1076	1064	1070	+	0,922
Spalt-like transcription factor 1	1082	1070	1076	+	0,961
Intestine specific homeodomain factor CDX-1	1087	1069	1078	-	0,961
Homeobox D10	1087	1071	1079	+	0,956
NK6 homeobox 1	1087	1073	1080	+	0,915
LIM-homeodomain transcription factor	1095	1073	1084	+	0,923
Muscle-specific Mt binding site	1095	1087	1091	-	0,902
THAP domain containing, apoptosis associated protein	1100	1090	1095	-	0,924
CCAAT/enhancer binding protein (C/EBP), epsilon	1103	1089	1096	-	0,974
Ets variant 1	1118	1098	1108	+	0,99
Signal transducer and activator of transcription 3	1121	1103	1112	-	0,959
Non-palindromic nuclear factor I binding sites	1127	1107	1117	+	0,995
AREB6 (Atp1a1 regulatory element binding factor 6)	1127	1115	1121	+	0,938
Interferon regulatory factor 1	1141	1117	1129	-	0,952
Barx2, homeobox transcription factor that preferentially binds to paired TAAT motifs	1171	1153	1162	+	0,973
Homeodomain transcription factor HOXC13	1170	1154	1162	-	0,922
Hematopoietically expressed homeobox, proline-rich homeodomain protein	1175	1157	1166	+	0,969
Interferon regulatory factor (IRF)-related protein (NF-EM5, PIP, LSIRF, ICSAT)	1179	1155	1167	-	0,958
NMP4 (nuclear matrix protein 4) / CIZ (Cas-interacting zinc finger protein)	1178	1168	1173	-	0,972
Special AT-rich sequence-binding protein 1, predominantly expressed in thymocytes, binds to matrix attachment regions (MARs)	1188	1174	1181	+	0,955
Barx2, homeobox transcription factor that preferentially binds to paired TAAT motifs	1193	1175	1184	+	0,953
NK6 homeobox 1	1191	1177	1184	+	0,925
Kruppel-like factor 7 (ubiquitous, UKLF) (secondary DNA binding preference)	1212	1194	1203	-	0,9
v-Myb, AMV v-myb	1215	1195	1205	+	0,907
T-Box factor 5 site (TBX5), mutations related to Holt-Oram syndrome	1220	1192	1206	+	0,99
AREB6 (Atp1a1 regulatory element binding factor 6)	1215	1203	1209	-	0,978
CCAAT/enhancer binding protein beta	1223	1209	1216	+	0,929
Nuclear factor Y (Y-box binding factor)	1229	1215	1222	+	0,923
TEA domain family member 4, TEF-3	1254	1242	1248	-	0,983
SRY (sex determining region Y)-box 1, dimeric binding sites	1280	1258	1269	-	0,901
Cytoplasmic polyadenylated homeobox	1290	1268	1279	+	0,95
GATA binding factor	1291	1279	1285	+	0,998

7.10 Table 4: Clinicopathological characteristics of the study population

N°	Sex	Age	Tumor site	Grading	T	N	M	Stage	Recurrance	Perineural invasion
1	M	76	scalp	G1	T1	Nx	M0	I	yes	ND
2	M	73	ear	G1	T1	Nx	M0	I	no	ND
3	F	86	cheek	ND	T2	Nx	M0	II	no	ND
4	M	68	ND	G1	T2	Nx	M0	II	no	ND
5	M	72	hand	G1	-	-	-	no staging	yes	ND
6	F	85	hand	G3	-	-	-	no staging	no	ND
7	M	67	hand	G2-G3	-	-	-	no staging	yes	ND
8	F	67	neck	G2	T3	Nx	M0	III	no	ND
9	F	71	ND	ND	T1	Nx	M0	I	no	ND
10	M	36	leg	G1	-	-	-	no staging	no	ND
11	M	49	leg	G2	-	-	-	no staging	no	ND
12	F	76	ND	G3	T2	Nx	M0	II	no	ND
13	F	76	lip	G2	T1	Nx	M0	I	no	ND
14	M	70	ear	G2	T1	Nx	M0	I	yes	ND
15	M	60	ND	G2	T2	Nx	M0	II	no	ND
16	M	67	cheek	G2-G3	T2	Nx	M0	II	no	ND
17	F	95	cheek	G2	T3	Nx	M0	III	no	ND
18	F	83	cheek	G2	T1	Nx	M0	I	no	ND
19	F	68	lip	G2	T1	Nx	M0	II	no	ND
20	M	79	scalp	G2	T3	Nx	M0	III	no	ND
21	F	51	arm	G2	-	-	-	no staging	no	ND
22	F	73	trunk	G3	-	-	-	no staging	no	yes
23	M	75	cheek	G2	T3	NX	M0	III	yes	no
24	M	77	forehead	G2-G3	T4	NX	M0	IV	no	no
25	M	77	scalp	ND	T1	NX	M0	I	yes	no
26	M	68	temple	G2	T3	NX	M0	III	no	yes
27	M	81	scalp	G2-G3	T2	NX	M0	II	yes	no
28	M	82	scalp	G2-G3	T3	NX	M0	III	yes	no
29	M	73	neck	G2	T3	NX	M0	III	yes	no
30	F	76	cheek	G1	T2	NX	M0	II	no	no
31	F	79	nose	G1	T1	NX	M0	I	no	no
32	M	69	cheek	G1	T1	NX	M0	I	yes	no
33	M	73	ear	G1	T1	NX	M0	I	no	no
34	M	81	scalp	G3	T3	NX	M0	III	no	no
35	M	71	scalp	G3	T3	N2	M0	IV	no	no
36	M	83	scalp	G1	T2	NX	M0	II	yes	no
37	M	67	ear	G3	T2	N2	M0	IV	yes	no
38	M	79	scalp	G1	T1	NX	M0	I	no	no
39	M	51	ear	G1	T2	NX	M0	II	no	no
40	M	86	forehead	G3	T2	NX	M0	II	yes	no
41	F	84	temple	G2-G3	T3	NX	M0	III	yes	no
42	F	82	temple	G2-G3	T3	NX	M0	III	no	no
43	M	75	neck	G3	T3	N1	M0	III	yes	yes
44	M	80	scalp	G2-G3	T1	Nx	M0	I	yes	no
45	M	77	ear	G2	T2	NX	M0	II	no	no
46	M	74	scalp	G2	T2	NX	M0	II	no	no
47	F	76	chin	G1	T3	NX	M0	III	no	no
48	M	83	forehead	G2	T3	NX	M0	III	yes	yes
49	M	61	scalp	ND	T2	NX	M0	II	yes	no
50	M	79	temple	G2	T3	NX	M0	III	yes	no
51	F	74	temple	G1	T1	NX	M0	I	no	no
52	M	68	scalp	G1-G2	T1	NX	M0	I	no	no
53	M	67	forehead	G3	T3	NX	M0	III	yes	yes
54	F	75	cheek	G1-G2	T2	NX	M0	II	no	no
55	M	75	scalp	G1-G2	T3	NX	M0	III	yes	no
56	M	85	scalp	G3	T3	NX	M0	III	yes	no
57	M	78	scalp	G3	T3	N0	M0	III	no	yes

58	M	86	cheek	G3	T3	NX	M0	III	no	yes
59	M	59	temple	G1-G2	T2	NX	M0	II	no	no
60	M	87	scalp	G1	T2	NX	M0	II	no	no
61	F	65	cheek	G3	T3	NX	M0	III	yes	yes
62	M	69	scalp	G1-G2	T1	NX	M0	I	no	no
63	M	78	ear	G1	T1	NX	M0	I	no	no
64	F	82	nose	G1	T1	NX	M0	I	no	no
65	M	86	scalp	G3	T3	NX	M0	III	no	yes
66	M	70	scalp	G1	T2	NX	M0	II	no	no
67	M	85	scalp	G3	T3	NX	M0	III	no	no
68	M	86	scalp	G3	T3	NX	M0	III	no	no
69	M	63	eyelid	G1	T1	NX	M0	I	no	no
70	F	86	nose	G1	T1	NX	M0	I	no	no
71	M	83	scalp	G2-G3	T3	NX	M0	III	no	no
72	F	87	forehead	G2	T3	N1	M1	IV	no	no

8. References

1. Dentice M, Luongo C, Huang S, Ambrosio R, Elefante A, Mirebeau-Prunier D, Zavacki AM, Fenzi G, Grachtchouk M, Hutchin M, Dlugosz AA, Bianco AC, Missero C, Larsen PR, Salvatore D. Sonic hedgehog-induced type 3 deiodinase blocks thyroid hormone action enhancing proliferation of normal and malignant keratinocytes. *Proc Natl Acad Sci U S A*. 2007;104(36):14466-14471.
2. Luongo C, Ambrosio R, Salzano S, Dlugosz AA, Missero C, Dentice M. The sonic hedgehog-induced type 3 deiodinase facilitates tumorigenesis of basal cell carcinoma by reducing Gli2 inactivation. *Endocrinology*. 2014;155(6):2077-2088.
3. Di Girolamo D, Ambrosio R, De Stefano MA, Mancino G, Porcelli T, Luongo C, Di Cicco E, Scalia G, Vecchio LD, Colao A, Dlugosz AA, Missero C, Salvatore D, Dentice M. Reciprocal interplay between thyroid hormone and microRNA-21 regulates hedgehog pathway-driven skin tumorigenesis. *J Clin Invest*. 2016;126(6):2308-2320.
4. Miro C, Di Cicco E, Ambrosio R, Mancino G, Di Girolamo D, Cicatiello AG, Sagliocchi S, Nappi A, De Stefano MA, Luongo C, Antonini D, Visconte F, Varricchio S, Ilardi G, Del Vecchio L, Staibano S, Boelen A, Blanpain C, Missero C, Salvatore D, Dentice M. Thyroid hormone induces progression and invasiveness of squamous cell carcinomas by promoting a ZEB-1/E-cadherin switch. *Nat Commun*. 2019;10(1):5410.
5. Mendoza A, Hollenberg AN. New insights into thyroid hormone action. *Pharmacol Ther*. 2017;173:135-145.
6. Bartalena L. Recent achievements in studies on thyroid hormone-binding proteins. *Endocr Rev*. 1990;11(1):47-64.
7. Nillni EA. Regulation of the hypothalamic thyrotropin releasing hormone (TRH) neuron by neuronal and peripheral inputs. *Front Neuroendocrinol*. 2010;31(2):134-156.
8. Visser WE, van Mullem AA, Jansen J, Visser TJ. The thyroid hormone transporters MCT8 and MCT10 transport the affinity-label N-bromoacetyl-[(125)I]T3 but are not modified by it. *Mol Cell Endocrinol*. 2011;337(1-2):96-100.
9. Visser WE, Friesema EC, Jansen J, Visser TJ. Thyroid hormone transport in and out of cells. *Trends Endocrinol Metab*. 2008;19(2):50-56.
10. Abe T, Kakyo M, Sakagami H, Tokui T, Nishio T, Tanemoto M, Nomura H, Hebert SC, Matsuno S, Kondo H, Yawo H. Molecular characterization and tissue distribution of a new organic anion transporter subtype (oatp3) that transports thyroid hormones and taurocholate and comparison with oatp2. *J Biol Chem*. 1998;273(35):22395-22401.
11. Schweizer U, Kohrle J. Function of thyroid hormone transporters in the central nervous system. *Biochim Biophys Acta*. 2013;1830(7):3965-3973.
12. Friesema EC, Ganguly S, Abdalla A, Manning Fox JE, Halestrap AP, Visser TJ. Identification of monocarboxylate transporter 8 as a specific thyroid hormone transporter. *J Biol Chem*. 2003;278(41):40128-40135.
13. Visser WE, Friesema EC, Visser TJ. Minireview: thyroid hormone transporters: the knowns and the unknowns. *Mol Endocrinol*. 2011;25(1):1-14.
14. Alkemade A, Vuijst CL, Unmehopa UA, Bakker O, Vennstrom B, Wiersinga WM, Swaab DF, Fliers E. Thyroid hormone receptor expression in the human

hypothalamus and anterior pituitary. *J Clin Endocrinol Metab*. 2005;90(2):904-912.
15. Alkemade A, Friesema EC, Unmehopa UA, Fabriek BO, Kuiper GG, Leonard JL, Wiersinga WM, Swaab DF, Visser TJ, Fliers E. Neuroanatomical pathways for thyroid hormone feedback in the human hypothalamus. *J Clin Endocrinol Metab*. 2005;90(7):4322-4334.
16. Heuer H, Maier MK, Iden S, Mittag J, Friesema EC, Visser TJ, Bauer K. The monocarboxylate transporter 8 linked to human psychomotor retardation is highly expressed in thyroid hormone-sensitive neuron populations. *Endocrinology*. 2005;146(4):1701-1706.
17. Curcio-Morelli C, Zavacki AM, Christofollete M, Gereben B, de Freitas BC, Harney JW, Li Z, Wu G, Bianco AC. Deubiquitination of type 2 iodothyronine deiodinase by von Hippel-Lindau protein-interacting deubiquitinating enzymes regulates thyroid hormone activation. *J Clin Invest*. 2003;112(2):189-196.
18. Sagar GD, Gereben B, Callebaut I, Mornon JP, Zeold A, Curcio-Morelli C, Harney JW, Luongo C, Mulcahey MA, Larsen PR, Huang SA, Bianco AC. The thyroid hormone-inactivating deiodinase functions as a homodimer. *Mol Endocrinol*. 2008;22(6):1382-1393.
19. Bianco AC, Salvatore D, Gereben B, Berry MJ, Larsen PR. Biochemistry, cellular and molecular biology, and physiological roles of the iodothyronine selenodeiodinases. *Endocr Rev*. 2002;23(1):38-89.
20. Gereben B, Goncalves C, Harney JW, Larsen PR, Bianco AC. Selective proteolysis of human type 2 deiodinase: a novel ubiquitin-proteasomal mediated mechanism for regulation of hormone activation. *Mol Endocrinol*. 2000;14(11):1697-1708.
21. Schneider MJ, Fiering SN, Thai B, Wu SY, St Germain E, Parlow AF, St Germain DL, Galton VA. Targeted disruption of the type 1 selenodeiodinase gene (Dio1) results in marked changes in thyroid hormone economy in mice. *Endocrinology*. 2006;147(1):580-589.
22. Burmeister LA, Pachucki J, St Germain DL. Thyroid hormones inhibit type 2 iodothyronine deiodinase in the rat cerebral cortex by both pre- and posttranslational mechanisms. *Endocrinology*. 1997;138(12):5231-5237.
23. Gereben B, Zeold A, Dentice M, Salvatore D, Bianco AC. Activation and inactivation of thyroid hormone by deiodinases: local action with general consequences. *Cell Mol Life Sci*. 2008;65(4):570-590.
24. Galton VA, Wood ET, St Germain EA, Withrow CA, Aldrich G, St Germain GM, Clark AS, St Germain DL. Thyroid hormone homeostasis and action in the type 2 deiodinase-deficient rodent brain during development. *Endocrinology*. 2007;148(7):3080-3088.
25. Refetoff S, Bassett JH, Beck-Peccoz P, Bernal J, Brent G, Chatterjee K, De Groot LJ, Dumitrescu AM, Jameson JL, Kopp PA, Murata Y, Persani L, Samarut J, Weiss RE, Williams GR, Yen PM. Classification and proposed nomenclature for inherited defects of thyroid hormone action, cell transport, and metabolism. *Thyroid*. 2014;24(3):407-409.
26. Proksch E, Brandner JM, Jensen JM. The skin: an indispensable barrier. *Exp Dermatol*. 2008;17(12):1063-1072.
27. Moll R, Divo M, Langbein L. The human keratins: biology and pathology. *Histochem Cell Biol*. 2008;129(6):705-733.

28. Antonini D, Sibilio A, Dentice M, Missero C. An Intimate Relationship between Thyroid Hormone and Skin: Regulation of Gene Expression. *Front Endocrinol (Lausanne)*. 2013;4:104.
29. Freinkel RK, Freinkel N. Hair growth and alopecia in hypothyroidism. *Arch Dermatol*. 1972;106(3):349-352.
30. Messenger AG. Thyroid hormone and hair growth. *Br J Dermatol*. 2000;142(4):633-634.
31. Slominski A, Wortsman J, Kohn L, Ain KB, Venkataraman GM, Pisarchik A, Chung JH, Giuliani C, Thornton M, Slugocki G, Tobin DJ. Expression of hypothalamic-pituitary-thyroid axis related genes in the human skin. *J Invest Dermatol*. 2002;119(6):1449-1455.
32. Cianfarani F, Baldini E, Cavalli A, Marchioni E, Lembo L, Teson M, Persechino S, Zambruno G, Ulisse S, Odorisio T, D'Armiento M. TSH receptor and thyroid-specific gene expression in human skin. *J Invest Dermatol*. 2010;130(1):93-101.
33. Daumerie C, Ludgate M, Costagliola S, Many MC. Evidence for thyrotropin receptor immunoreactivity in pretibial connective tissue from patients with thyroid-associated dermopathy. *Eur J Endocrinol*. 2002;146(1):35-38.
34. Slominski A, Wortsman J, Tuckey RC, Paus R. Differential expression of HPA axis homolog in the skin. *Mol Cell Endocrinol*. 2007;265-266:143-149.
35. Billoni N, Buan B, Gautier B, Gaillard O, Mahe YF, Bernard BA. Thyroid hormone receptor beta1 is expressed in the human hair follicle. *Br J Dermatol*. 2000;142(4):645-652.
36. Martinez-Iglesias O, Garcia-Silva S, Tenbaum SP, Regadera J, Larcher F, Paramio JM, Vennstrom B, Aranda A. Thyroid hormone receptor beta1 acts as a potent suppressor of tumor invasiveness and metastasis. *Cancer Res*. 2009;69(2):501-509.
37. Ahsan MK, Urano Y, Kato S, Oura H, Arase S. Immunohistochemical localization of thyroid hormone nuclear receptors in human hair follicles and in vitro effect of L-triiodothyronine on cultured cells of hair follicles and skin. *J Med Invest*. 1998;44(3-4):179-184.
38. Luongo C, Dentice M, Salvatore D. Deiodinases and their intricate role in thyroid hormone homeostasis. *Nat Rev Endocrinol*. 2019;15(8):479-488.
39. Jho SH, Radoja N, Im MJ, Tomic-Canic M. Negative response elements in keratin genes mediate transcriptional repression and the cross-talk among nuclear receptors. *J Biol Chem*. 2001;276(49):45914-45920.
40. Radoja N, Diaz DV, Minars TJ, Freedberg IM, Blumenberg M, Tomic-Canic M. Specific organization of the negative response elements for retinoic acid and thyroid hormone receptors in keratin gene family. *J Invest Dermatol*. 1997;109(4):566-572.
41. Radoja N, Stojadinovic O, Waseem A, Tomic-Canic M, Milisavljevic V, Teebor S, Blumenberg M. Thyroid hormones and gamma interferon specifically increase K15 keratin gene transcription. *Mol Cell Biol*. 2004;24(8):3168-3179.
42. Ramot Y, Paus R, Tiede S, Zlotogorski A. Endocrine controls of keratin expression. *Bioessays*. 2009;31(4):389-399.
43. Safer JD, Crawford TM, Holick MF. A role for thyroid hormone in wound healing through keratin gene expression. *Endocrinology*. 2004;145(5):2357-2361.
44. Safer JD, Crawford TM, Holick MF. Topical thyroid hormone accelerates wound healing in mice. *Endocrinology*. 2005;146(10):4425-4430.

45. Safer JD, Colan SD, Fraser LM, Wondisford FE. A pituitary tumor in a patient with thyroid hormone resistance: a diagnostic dilemma. *Thyroid*. 2001;11(3):281-291.
46. Mancino G, Sibilio A, Luongo C, Di Cicco E, Miro C, Cicatiello AG, Nappi A, Sagliocchi S, Ambrosio R, De Stefano MA, Di Girolamo D, Porcelli T, Murolo M, Saracino F, Perruolo G, Formisano P, Stornaiuolo M, Dentice M. The Thyroid Hormone Inactivator Enzyme, Type 3 Deiodinase, Is Essential for Coordination of Keratinocyte Growth and Differentiation. *Thyroid*. 2020;30(7):1066-1078.
47. Safer JD. Thyroid hormone and wound healing. *J Thyroid Res*. 2013;2013:124538.
48. Safer JD, Crawford TM, Fraser LM, Hoa M, Ray S, Chen TC, Persons K, Holick MF. Thyroid hormone action on skin: diverging effects of topical versus intraperitoneal administration. *Thyroid*. 2003;13(2):159-165.
49. Leonhardt JM, Heymann WR. Thyroid disease and the skin. *Dermatol Clin*. 2002;20(3):473-481, vii.
50. Leiter U, Eigentler T, Garbe C. Epidemiology of skin cancer. *Adv Exp Med Biol*. 2014;810:120-140.
51. Karimkhani C, Boyers LN, Dellavalle RP, Weinstock MA. It's time for "keratinocyte carcinoma" to replace the term "nonmelanoma skin cancer". *J Am Acad Dermatol*. 2015;72(1):186-187.
52. Karia PS, Han J, Schmults CD. Cutaneous squamous cell carcinoma: estimated incidence of disease, nodal metastasis, and deaths from disease in the United States, 2012. *J Am Acad Dermatol*. 2013;68(6):957-966.
53. Schmults CD, Karia PS, Carter JB, Han J, Qureshi AA. Factors predictive of recurrence and death from cutaneous squamous cell carcinoma: a 10-year, single-institution cohort study. *JAMA Dermatol*. 2013;149(5):541-547.
54. Rees JR, Zens MS, Celaya MO, Riddle BL, Karagas MR, Peacock JL. Survival after squamous cell and basal cell carcinoma of the skin: A retrospective cohort analysis. *Int J Cancer*. 2015;137(4):878-884.
55. Robinson JK, Dahiya M. Basal cell carcinoma with pulmonary and lymph node metastasis causing death. *Arch Dermatol*. 2003;139(5):643-648.
56. Yilmaz AS, Ozer HG, Gillespie JL, Allain DC, Bernhardt MN, Furlan KC, Castro LT, Peters SB, Nagarajan P, Kang SY, Iwenofu OH, Olencki T, Teknos TN, Toland AE. Differential mutation frequencies in metastatic cutaneous squamous cell carcinomas versus primary tumors. *Cancer*. 2017;123(7):1184-1193.
57. Pickering CR, Zhou JH, Lee JJ, Drummond JA, Peng SA, Saade RE, Tsai KY, Curry JL, Tetzlaff MT, Lai SY, Yu J, Muzny DM, Doddapaneni H, Shinbrot E, Covington KR, Zhang J, Seth S, Caulin C, Clayman GL, El-Naggar AK, Gibbs RA, Weber RS, Myers JN, Wheeler DA, Frederick MJ. Mutational landscape of aggressive cutaneous squamous cell carcinoma. *Clin Cancer Res*. 2014;20(24):6582-6592.
58. Pickering CR, Zhang J, Neskey DM, Zhao M, Jasser SA, Wang J, Ward A, Tsai CJ, Ortega Alves MV, Zhou JH, Drummond J, El-Naggar AK, Gibbs R, Weinstein JN, Wheeler DA, Wang J, Frederick MJ, Myers JN. Squamous cell carcinoma of the oral tongue in young non-smokers is genomically similar to tumors in older smokers. *Clin Cancer Res*. 2014;20(14):3842-3848.
59. Al-Rohil RN, Tarasen AJ, Carlson JA, Wang K, Johnson A, Yelensky R, Lipson D, Elvin JA, Vergilio JA, Ali SM, Suh J, Miller VA, Stephens PJ, Ganesan P,

Janku F, Karp DD, Subbiah V, Mihm MC, Ross JS. Evaluation of 122 advanced-stage cutaneous squamous cell carcinomas by comprehensive genomic profiling opens the door for new routes to targeted therapies. *Cancer*. 2016;122(2):249-257.

60. Bonilla X, Parmentier L, King B, Bezrukov F, Kaya G, Zoete V, Seplyarskiy VB, Sharpe HJ, McKee T, Letourneau A, Ribaux PG, Popadin K, Basset-Seguin N, Ben Chaabene R, Santoni FA, Andrianova MA, Guipponi M, Garieri M, Verdan C, Grosdemange K, Sumara O, Eilers M, Aifantis I, Michielin O, de Sauvage FJ, Antonarakis SE, Nikolaev SI. Genomic analysis identifies new drivers and progression pathways in skin basal cell carcinoma. *Nat Genet*. 2016;48(4):398-406.
61. Nagarajan P, Asgari MM, Green AC, Guhan SM, Arron ST, Proby CM, Rollison DE, Harwood CA, Toland AE. Keratinocyte Carcinomas: Current Concepts and Future Research Priorities. *Clin Cancer Res*. 2019;25(8):2379-2391.
62. Alam M, Ratner D. Cutaneous squamous-cell carcinoma. *N Engl J Med*. 2001;344(13):975-983.
63. Cockerell CJ. Histopathology of incipient intraepidermal squamous cell carcinoma ("actinic keratosis"). *J Am Acad Dermatol*. 2000;42(1 Pt 2):11-17.
64. Owens DM, Watt FM. Contribution of stem cells and differentiated cells to epidermal tumours. *Nat Rev Cancer*. 2003;3(6):444-451.
65. Kemp CJ. Multistep skin cancer in mice as a model to study the evolution of cancer cells. *Semin Cancer Biol*. 2005;15(6):460-473.
66. Quintanilla M, Brown K, Ramsden M, Balmain A. Carcinogen-specific mutation and amplification of Ha-ras during mouse skin carcinogenesis. *Nature*. 1986;322(6074):78-80.
67. Spencer JM, Kahn SM, Jiang W, DeLeo VA, Weinstein IB. Activated ras genes occur in human actinic keratoses, premalignant precursors to squamous cell carcinomas. *Arch Dermatol*. 1995;131(7):796-800.
68. Sutter C, Strickland PT, Mukhtar H, Agarwal R, Winter H, Schweizer J. ras gene activation and aberrant expression of keratin K13 in ultraviolet B radiation-induced epidermal neoplasias of mouse skin. *Mol Carcinog*. 1993;8(1):13-19.
69. Perez-Losada J, Balmain A. Stem-cell hierarchy in skin cancer. *Nat Rev Cancer*. 2003;3(6):434-443.
70. Pastushenko I, Brisebarre A, Sifrim A, Fioramonti M, Revenco T, Boumahdi S, Van Keymeulen A, Brown D, Moers V, Lemaire S, De Clercq S, Minguijon E, Balsat C, Sokolow Y, Dubois C, De Cock F, Scozzaro S, Sopena F, Lanas A, D'Haene N, Salmon I, Marine JC, Voet T, Sotiropoulou PA, Blanpain C. Identification of the tumour transition states occurring during EMT. *Nature*. 2018;556(7702):463-468.
71. Mani SA, Guo W, Liao MJ, Eaton EN, Ayyanan A, Zhou AY, Brooks M, Reinhard F, Zhang CC, Shipitsin M, Campbell LL, Polyak K, Brisken C, Yang J, Weinberg RA. The epithelial-mesenchymal transition generates cells with properties of stem cells. *Cell*. 2008;133(4):704-715.
72. Morel AP, Lievre M, Thomas C, Hinkal G, Ansieau S, Puisieux A. Generation of breast cancer stem cells through epithelial-mesenchymal transition. *PLoS One*. 2008;3(8):e2888.
73. Alonso L, Fuchs E. Stem cells of the skin epithelium. *Proc Natl Acad Sci U S A*. 2003;100 Suppl 1:11830-11835.

74. Blanpain C, Fuchs E. Stem cell plasticity. Plasticity of epithelial stem cells in tissue regeneration. *Science*. 2014;344(6189):1242281.
75. Taylor G, Lehrer MS, Jensen PJ, Sun TT, Lavker RM. Involvement of follicular stem cells in forming not only the follicle but also the epidermis. *Cell*. 2000;102(4):451-461.
76. Blanpain C, Fuchs E. Epidermal homeostasis: a balancing act of stem cells in the skin. *Nat Rev Mol Cell Biol*. 2009;10(3):207-217.
77. Pattabiraman DR, Weinberg RA. Tackling the cancer stem cells - what challenges do they pose? *Nat Rev Drug Discov*. 2014;13(7):497-512.
78. Clarke MF, Dick JE, Dirks PB, Eaves CJ, Jamieson CH, Jones DL, Visvader J, Weissman IL, Wahl GM. Cancer stem cells--perspectives on current status and future directions: AACR Workshop on cancer stem cells. *Cancer Res*. 2006;66(19):9339-9344.
79. Beck B, Blanpain C. Unravelling cancer stem cell potential. *Nat Rev Cancer*. 2013;13(10):727-738.
80. Nassar D, Blanpain C. Cancer Stem Cells: Basic Concepts and Therapeutic Implications. *Annu Rev Pathol*. 2016;11:47-76.
81. Li C, Heidt DG, Dalerba P, Burant CF, Zhang L, Adsay V, Wicha M, Clarke MF, Simeone DM. Identification of pancreatic cancer stem cells. *Cancer Res*. 2007;67(3):1030-1037.
82. Prince ME, Sivanandan R, Kaczorowski A, Wolf GT, Kaplan MJ, Dalerba P, Weissman IL, Clarke MF, Ailles LE. Identification of a subpopulation of cells with cancer stem cell properties in head and neck squamous cell carcinoma. *Proc Natl Acad Sci U S A*. 2007;104(3):973-978.
83. Vermeulen L, Todaro M, de Sousa Mello F, Sprick MR, Kemper K, Perez Alea M, Richel DJ, Stassi G, Medema JP. Single-cell cloning of colon cancer stem cells reveals a multi-lineage differentiation capacity. *Proc Natl Acad Sci U S A*. 2008;105(36):13427-13432.
84. Schatton T, Murphy GF, Frank NY, Yamaura K, Waaga-Gasser AM, Gasser M, Zhan Q, Jordan S, Duncan LM, Weishaupt C, Fuhlbrigge RC, Kupper TS, Sayegh MH, Frank MH. Identification of cells initiating human melanomas. *Nature*. 2008;451(7176):345-349.
85. Malanchi I, Peinado H, Kassen D, Hussenet T, Metzger D, Chambon P, Huber M, Hohl D, Cano A, Birchmeier W, Huelsken J. Cutaneous cancer stem cell maintenance is dependent on beta-catenin signalling. *Nature*. 2008;452(7187):650-653.
86. Beatson GT. On the Treatment of Inoperable Cases of Carcinoma of the Mamma: Suggestions for a New Method of Treatment, with Illustrative Cases. *Trans Med Chir Soc Edinb*. 1896;15:153-179.
87. Meyer EL, Wagner MS, Maia AL. [Iodothyronine deiodinases expression in thyroid neoplasias]. *Arq Bras Endocrinol Metabol*. 2007;51(5):690-700.
88. Piekielko-Witkowska A, Nauman A. Iodothyronine deiodinases and cancer. *J Endocrinol Invest*. 2011;34(9):716-728.
89. Casula S, Bianco AC. Thyroid hormone deiodinases and cancer. *Front Endocrinol (Lausanne)*. 2012;3:74.
90. Dentice M, Antonini D, Salvatore D. Type 3 deiodinase and solid tumors: an intriguing pair. *Expert Opin Ther Targets*. 2013;17(11):1369-1379.

91. Huang SA, Tu HM, Harney JW, Venihaki M, Butte AJ, Kozakewich HP, Fishman SJ, Larsen PR. Severe hypothyroidism caused by type 3 iodothyronine deiodinase in infantile hemangiomas. *N Engl J Med*. 2000;343(3):185-189.
92. Huang SA, Fish SA, Dorfman DM, Salvatore D, Kozakewich HP, Mandel SJ, Larsen PR. A 21-year-old woman with consumptive hypothyroidism due to a vascular tumor expressing type 3 iodothyronine deiodinase. *J Clin Endocrinol Metab*. 2002;87(10):4457-4461.
93. Weber Pasa M, Selbach Scheffel R, Borsatto Zanella A, Maia AL, Dora JM. Consumptive Hypothyroidism: Case Report of Hepatic Hemangioendotheliomas Successfully Treated with Vincristine and Systematic Review of the Syndrome. *Eur Thyroid J*. 2017;6(6):321-327.
94. Miro C, Ambrosio R, De Stefano MA, Di Girolamo D, Di Cicco E, Cicatiello AG, Mancino G, Porcelli T, Raia M, Del Vecchio L, Salvatore D, Dentice M. The Concerted Action of Type 2 and Type 3 Deiodinases Regulates the Cell Cycle and Survival of Basal Cell Carcinoma Cells. *Thyroid*. 2017;27(4):567-576.
95. Aw DK, Sinha RA, Tan HC, Loh LM, Salvatore D, Yen PM. Studies of molecular mechanisms associated with increased deiodinase 3 expression in a case of consumptive hypothyroidism. *J Clin Endocrinol Metab*. 2014;99(11):3965-3971.
96. Kaplan MM, Pan CY, Gordon PR, Lee JK, Gilchrest BA. Human epidermal keratinocytes in culture convert thyroxine to 3,5,3'-triiodothyronine by type II iodothyronine deiodination: a novel endocrine function of the skin. *J Clin Endocrinol Metab*. 1988;66(4):815-822.
97. Santini F, Vitti P, Chiovato L, Ceccarini G, Macchia M, Montanelli L, Gatti G, Rosellini V, Mammoli C, Martino E, Chopra IJ, Safer JD, Braverman LE, Pinchera A. Role for inner ring deiodination preventing transcutaneous passage of thyroxine. *J Clin Endocrinol Metab*. 2003;88(6):2825-2830.
98. Sellheyer K. Basal cell carcinoma: cell of origin, cancer stem cell hypothesis and stem cell markers. *Br J Dermatol*. 2011;164(4):696-711.
99. Mori K, Yoshida K, Kayama T, Kaise N, Fukazawa H, Kiso Y, Kikuchi K, Aizawa Y, Abe K. Thyroxine 5-deiodinase in human brain tumors. *J Clin Endocrinol Metab*. 1993;77(5):1198-1202.
100. Murakami M, Araki O, Morimura T, Hosoi Y, Mizuma H, Yamada M, Kurihara H, Ishiuchi S, Tamura M, Sasaki T, Mori M. Expression of type II iodothyronine deiodinase in brain tumors. *J Clin Endocrinol Metab*. 2000;85(11):4403-4406.
101. Nauman P, Bonicki W, Michalik R, Warzecha A, Czernicki Z. The concentration of thyroid hormones and activities of iodothyronine deiodinases are altered in human brain gliomas. *Folia Neuropathol*. 2004;42(2):67-73.
102. Canettieri G, Celi FS, Baccheschi G, Salvatori L, Andreoli M, Centanni M. Isolation of human type 2 deiodinase gene promoter and characterization of a functional cyclic adenosine monophosphate response element. *Endocrinology*. 2000;141(5):1804-1813.
103. Curcio C, Baqui MM, Salvatore D, Rihn BH, Mohr S, Harney JW, Larsen PR, Bianco AC. The human type 2 iodothyronine deiodinase is a selenoprotein highly expressed in a mesothelioma cell line. *J Biol Chem*. 2001;276(32):30183-30187.
104. Gouveia CH, Christoffolete MA, Zaitune CR, Dora JM, Harney JW, Maia AL, Bianco AC. Type 2 iodothyronine selenodeiodinase is expressed throughout the mouse skeleton and in the MC3T3-E1 mouse osteoblastic cell line during differentiation. *Endocrinology*. 2005;146(1):195-200.

105. Chambers I, Silva J, Colby D, Nichols J, Nijmeijer B, Robertson M, Vrana J, Jones K, Grotewold L, Smith A. Nanog safeguards pluripotency and mediates germline development. *Nature*. 2007;450(7173):1230-1234.
106. Mitsui K, Tokuzawa Y, Itoh H, Segawa K, Murakami M, Takahashi K, Maruyama M, Maeda M, Yamanaka S. The homeoprotein Nanog is required for maintenance of pluripotency in mouse epiblast and ES cells. *Cell*. 2003;113(5):631-642.
107. Loh YH, Wu Q, Chew JL, Vega VB, Zhang W, Chen X, Bourque G, George J, Leong B, Liu J, Wong KY, Sung KW, Lee CW, Zhao XD, Chiu KP, Lipovich L, Kuznetsov VA, Robson P, Stanton LW, Wei CL, Ruan Y, Lim B, Ng HH. The Oct4 and Nanog transcription network regulates pluripotency in mouse embryonic stem cells. *Nat Genet*. 2006;38(4):431-440.
108. Wang J, Rao S, Chu J, Shen X, Levasseur DN, Theunissen TW, Orkin SH. A protein interaction network for pluripotency of embryonic stem cells. *Nature*. 2006;444(7117):364-368.
109. Piazzolla D, Palla AR, Pantoja C, Canamero M, de Castro IP, Ortega S, Gomez-Lopez G, Dominguez O, Megias D, Roncador G, Luque-Garcia JL, Fernandez-Tresguerres B, Fernandez AF, Fraga MF, Rodriguez-Justo M, Manzanares M, Sanchez-Carbayo M, Garcia-Pedrero JM, Rodrigo JP, Malumbres M, Serrano M. Lineage-restricted function of the pluripotency factor NANOG in stratified epithelia. *Nat Commun*. 2014;5:4226.
110. Palla AR, Piazzolla D, Alcazar N, Canamero M, Grana O, Gomez-Lopez G, Dominguez O, Duenas M, Paramio JM, Serrano M. The pluripotency factor NANOG promotes the formation of squamous cell carcinomas. *Sci Rep*. 2015;5:10205.
111. Iv Santaliz-Ruiz LE, Xie X, Old M, Teknos TN, Pan Q. Emerging role of nanog in tumorigenesis and cancer stem cells. *Int J Cancer*. 2014;135(12):2741-2748.
112. de Vicente JC, Rodriguez-Santamarta T, Rodrigo JP, Allonca E, Vallina A, Singhania A, Donate-Perez Del Molino P, Garcia-Pedrero JM. The Emerging Role of NANOG as an Early Cancer Risk Biomarker in Patients with Oral Potentially Malignant Disorders. *J Clin Med*. 2019;8(9).
113. Rodrigo JP, Villaronga MA, Menendez ST, Hermida-Prado F, Quer M, Vilaseca I, Allonca E, Pedregal Mallo D, Astudillo A, Garcia-Pedrero JM. A Novel Role For Nanog As An Early Cancer Risk Marker In Patients With Laryngeal Precancerous Lesions. *Sci Rep*. 2017;7(1):11110.
114. Qin S, Li Y, Cao X, Du J, Huang X. NANOG regulates epithelial-mesenchymal transition and chemoresistance in ovarian cancer. *Biosci Rep*. 2017;37(1).
115. Krashin E, Piekielko-Witkowska A, Ellis M, Ashur-Fabian O. Thyroid Hormones and Cancer: A Comprehensive Review of Preclinical and Clinical Studies. *Front Endocrinol (Lausanne)*. 2019;10:59.
116. Pinto M, Soares P, Ribatti D. Thyroid hormone as a regulator of tumor induced angiogenesis. *Cancer Lett*. 2011;301(2):119-126.
117. Davis PJ, Sudha T, Lin HY, Mousa SA. Thyroid Hormone, Hormone Analogs, and Angiogenesis. *Compr Physiol*. 2015;6(1):353-362.
118. Cremaschi GA, Cayrol F, Sterle HA, Diaz Flaque MC, Barreiro Arcos ML. Thyroid hormones and their membrane receptors as therapeutic targets for T cell lymphomas. *Pharmacol Res*. 2016;109:55-63.
119. Lin HY, Chin YT, Yang YC, Lai HY, Wang-Peng J, Liu LF, Tang HY, Davis PJ. Thyroid Hormone, Cancer, and Apoptosis. *Compr Physiol*. 2016;6(3):1221-1237.

120. Shinderman-Maman E, Cohen K, Weingarten C, Nabriski D, Twito O, Baraf L, Hercbergs A, Davis PJ, Werner H, Ellis M, Ashur-Fabian O. The thyroid hormone-alphavbeta3 integrin axis in ovarian cancer: regulation of gene transcription and MAPK-dependent proliferation. *Oncogene*. 2016;35(15):1977-1987.
121. Chin YT, Wei PL, Ho Y, Nana AW, Changou CA, Chen YR, Yang YS, Hsieh MT, Hercbergs A, Davis PJ, Shih YJ, Lin HY. Thyroxine inhibits resveratrol-caused apoptosis by PD-L1 in ovarian cancer cells. *Endocr Relat Cancer*. 2018;25(5):533-545.
122. Schmidinger M, Vogl UM, Bojic M, Lamm W, Heinzl H, Haitel A, Clodi M, Kramer G, Zielinski CC. Hypothyroidism in patients with renal cell carcinoma: blessing or curse? *Cancer*. 2011;117(3):534-544.
123. Bailey EB, Tantravahi SK, Poole A, Agarwal AM, Straubhar AM, Batten JA, Patel SB, Wells CE, Stenehjem DD, Agarwal N. Correlation of degree of hypothyroidism with survival outcomes in patients with metastatic renal cell carcinoma receiving vascular endothelial growth factor receptor tyrosine kinase inhibitors. *Clin Genitourin Cancer*. 2015;13(3):e131-137.
124. Cristofanilli M, Yamamura Y, Kau SW, Bevers T, Strom S, Patangan M, Hsu L, Krishnamurthy S, Theriault RL, Hortobagyi GN. Thyroid hormone and breast carcinoma. Primary hypothyroidism is associated with a reduced incidence of primary breast carcinoma. *Cancer*. 2005;103(6):1122-1128.
125. Nelson M, Hercbergs A, Rybicki L, Strome M. Association between development of hypothyroidism and improved survival in patients with head and neck cancer. *Arch Otolaryngol Head Neck Surg*. 2006;132(10):1041-1046.
126. Puhr HC, Wolf P, Berghoff AS, Schoppmann SF, Preusser M, Ilhan-Mutlu A. Elevated Free Thyroxine Levels Are Associated with Poorer Overall Survival in Patients with Gastroesophageal Cancer: A Retrospective Single Center Analysis. *Horm Cancer*. 2020;11(1):42-51.
127. Huang PY, Balmain A. Modeling cutaneous squamous carcinoma development in the mouse. *Cold Spring Harb Perspect Med*. 2014;4(9):a013623.
128. Castagna MG, Dentice M, Cantara S, Ambrosio R, Maino F, Porcelli T, Marzocchi C, Garbi C, Pacini F, Salvatore D. DIO2 Thr92Ala Reduces Deiodinase-2 Activity and Serum-T3 Levels in Thyroid-Deficient Patients. *J Clin Endocrinol Metab*. 2017;102(5):1623-1630.
129. Tomakidi P, Stark HJ, Herold-Mende C, Bosch FX, Steinbauer H, Fusenig NE, Breitkreutz D. Discriminating expression of differentiation markers evolves in transplants of benign and malignant human skin keratinocytes through stromal interactions. *J Pathol*. 2003;200(3):298-307.
130. Lapouge G, Beck B, Nassar D, Dubois C, Dekoninck S, Blanpain C. Skin squamous cell carcinoma propagating cells increase with tumour progression and invasiveness. *EMBO J*. 2012;31(24):4563-4575.
131. Sheng H, Goich S, Wang A, Grachtchouk M, Lowe L, Mo R, Lin K, de Sauvage FJ, Sasaki H, Hui CC, Dlugosz AA. Dissecting the oncogenic potential of Gli2: deletion of an NH(2)-terminal fragment alters skin tumor phenotype. *Cancer Res*. 2002;62(18):5308-5316.
132. Vasioukhin V, Degenstein L, Wise B, Fuchs E. The magical touch: genome targeting in epidermal stem cells induced by tamoxifen application to mouse skin. *Proc Natl Acad Sci U S A*. 1999;96(15):8551-8556.

133. Wong SY, Seol AD, So PL, Ermilov AN, Bichakjian CK, Epstein EH, Jr., Dlugosz AA, Reiter JF. Primary cilia can both mediate and suppress Hedgehog pathway-dependent tumorigenesis. *Nat Med*. 2009;15(9):1055-1061.
134. Peterson SC, Eberl M, Vagnozzi AN, Belkadi A, Veniaminova NA, Verhaegen ME, Bichakjian CK, Ward NL, Dlugosz AA, Wong SY. Basal cell carcinoma preferentially arises from stem cells within hair follicle and mechanosensory niches. *Cell Stem Cell*. 2015;16(4):400-412.
135. Youssef KK, Van Keymeulen A, Lapouge G, Beck B, Michaux C, Achouri Y, Sotiropoulou PA, Blanpain C. Identification of the cell lineage at the origin of basal cell carcinoma. *Nat Cell Biol*. 2010;12(3):299-305.
136. Brabletz S, Brabletz T. The ZEB/miR-200 feedback loop--a motor of cellular plasticity in development and cancer? *EMBO Rep*. 2010;11(9):670-677.
137. Caramel J, Ligier M, Puisieux A. Pleiotropic Roles for ZEB1 in Cancer. *Cancer Res*. 2018;78(1):30-35.
138. Camp RL, Dolled-Filhart M, Rimm DL. X-tile: a new bio-informatics tool for biomarker assessment and outcome-based cut-point optimization. *Clin Cancer Res*. 2004;10(21):7252-7259.
139. Cohen J, Chen Z, Lu SL, Yang XP, Arun P, Ehsanian R, Brown MS, Lu H, Yan B, Diallo O, Wang XJ, Van Waes C. Attenuated transforming growth factor beta signaling promotes nuclear factor-kappaB activation in head and neck cancer. *Cancer Res*. 2009;69(8):3415-3424.
140. Chung CH, Parker JS, Karaca G, Wu J, Funkhouser WK, Moore D, Butterfoss D, Xiang D, Zanation A, Yin X, Shockley WW, Weissler MC, Dressler LG, Shores CG, Yarbrough WG, Perou CM. Molecular classification of head and neck squamous cell carcinomas using patterns of gene expression. *Cancer Cell*. 2004;5(5):489-500.
141. Heppner GH, Miller FR. The cellular basis of tumor progression. *Int Rev Cytol*. 1998;177:1-56.
142. Talmadge JE, Wolman SR, Fidler IJ. Evidence for the clonal origin of spontaneous metastases. *Science*. 1982;217(4557):361-363.
143. Liu S, Sun J, Cai B, Xi X, Yang L, Zhang Z, Feng Y, Sun Y. NANOG regulates epithelial-mesenchymal transition and chemoresistance through activation of the STAT3 pathway in epithelial ovarian cancer. *Tumour Biol*. 2016;37(7):9671-9680.
144. Jeter CR, Yang T, Wang J, Chao HP, Tang DG. Concise Review: NANOG in Cancer Stem Cells and Tumor Development: An Update and Outstanding Questions. *Stem Cells*. 2015;33(8):2381-2390.
145. Palla AR, Piazzolla D, Abad M, Li H, Dominguez O, Schonthaler HB, Wagner EF, Serrano M. Reprogramming activity of NANOGP8, a NANOG family member widely expressed in cancer. *Oncogene*. 2014;33(19):2513-2519.